Schlumberger Oilfield Australia Pty Limited
A.C.N. 003 264 597
Level 5, 256 St Georges Terrace
Perth WA 6000
Ph: (08) 9420 4800 Fax: (08) 9322 3080

ESSO AUSTRALIA LTD

WELL SEISMIC PROCESSING REPORT

Vertical Incidence VSP

BLACKBACK A1 ST-1

FIELD: BLACKBACK

COUNTRY: AUSTRALIA

COORDINATES: 038 32' 31.677" S
: 148 33' 11.274" E

DATE OF VSP SURVEY: 18/21-April 1999

REFERENCE NO:

INTERVAL: 4440 - 421 m MD

Prepared by Henry Cao

CONTENTS

List of Tables

List of Figures

1. Introduction

A borehole seismic survey was conducted using Combinable Seismic Imager (CSI) tools at the *Blackback A1 ST-1 (BBA1ST-1)* well. The survey was carried out between 18 and 21 April, 1999.

The borehole seismic program consists of three parts: a velocity survey for the water column, a wireline conveyed vertical incidence VSP (VIVSP) and a TLC conveyed VIVSP. The water velocity was obtained by measuring the transit time between the source and the receiver at the sea bottom. The wireline conveyed VIVSP covers a measured depth range of 1312 – 1912 m. The TLC conveyed VIVSP covers a measured depth range of 3144.5 – 4440 m.

The borehole seismic data were edited and processed using the borehole seismic package of GeoFrame 3.5 which was commercially released from Schlumberger Austin Systems Center.

This report describes the processing of the borehole seismic surveys.

2. Data Acquisition

The objectives of the Blackback A1 ST-1 (BBA1ST-1) borehole seismic survey were as follows:

- Accurate time-depth conversion table for surface seismic events intersecting the well trajectory
- Good average velocity above the well trajectory
- Reflection imaging below the well trajectory

The downhole tools for the survey were the Combinable Seismic Imager (CSI, also called CSAT – Combinable Seismic Acquisition Tool) fitted with gimballed SM4 geophones. The CSI has its sensor module acoustically decoupled from the tool house and this unique separation prevents the signal distortion caused by coupling resonance and modal resonance results from the size and mass of conventional openhole VSP tools. For seismic acquisition, the CSI tool is anchored against the formation. Then the sensor module is decoupled from the main body of the tool and held firmly against the borehole wall. Optimum placement of the sensor module is verified by the response of each geophone to mechanical excitation generated by the shaker in the module. The decoupled sensor module uses the large acquisition cartridge in the tool body for powerful downhole signal processing and quality control without being adversely affected by any tool body vibrations.

In addition to its high accuracy, the CSI tool is extremely versatile. Because the decoupled design allows running long tool strings without acoustical degradation, an array of several CSI tools can be used to obtain rapid multilevel seismic arrays. The CSI tool is also compatible with other tools for positioning and correlation measurements.

The data was acquired in several logging attempts. The first wireline attempt was made with tail guiding DLEs and flex joints electrically decoupled from the CSAT. Calibration shots were recorded at 421 and 1312 m MD. The toolstring could not pass 1312 m MD.

The second wireline attempt was made with HRMS added to tail and flex joints removed. The toolstring could not pass 1530 m MD due to too much drag. The third wireline attempt was made with one more HRMS added and the hole finder and tool turners removed. The toolstring could not pass 1930 m MD. VIVSP was recorded from 1912 to 1320 m MD.

Toolstring was reconfigured for TLC run: second CSAT, AMS, swivel, tool turners and DWCH were added. Toolstring was run blindly in open hole from 1302 to 3150 m MD on ESSO's request. Compression on toolstring could not be monitored due to very high drag on drill pipe. VIVSP was recorded with both CSATs in TLC from 4440 to 3150 m MD (maximum interval possible with one latch). Noisy signal was recorded at 3360 m MD. Checkshots were recorded above 3360 m MD as per ESSO request.

For easy reference, the VSP data acquired on wireline will be referred to as Run-1 and the data acquired on TLC will be referred to as Run-2 in subsequent descriptions.

A G-type airgun of 150 cc was used as the seismic energy source. The gun was fired at 120 bar with compressed nitrogen bottles. The gun was positioned 6 meter below the mean sea level (MSL) and a hydrophone was directly above the gun and 3 m below MSL. A supply boat was used to tow the gun to the position approximately directly above the downhole CSAT. Gun positions were navigated by FUGRO using a differential GPS system. The communication between the supply boat and the MAXIS logging unit was established by a MACHA radio system.

Recording was made on the Schlumberger Maxis 500 Unit and data were saved in the DLIS format. A copy of the seismic data in SEGY format was made at the wellsite and immediately delivered to ESSO Australia.

2.1 Well deviation

Well deviation data was acquired during drilling and is attached here as Appendix A. The well is vertical until it starts to deviate at about 800 m MD. At around 1280 m MD, the well deviation reaches 60 degrees and remains fairly constant till TD of 4695 m MD. In the deviated section of the well, the well azimuth keeps at 355 degrees from the North. Figures 1 and 2 show the well deviation and azimuthal data. X-Y (Easting and Northing with the wellhead as the origin) and Sagittal (azimuthal) planes of downhole geophones are displayed in Figures 3 and 4.

2.2 VSP acquisition geometry

The VSP survey parameters are listed in Table 1. Important raw geometry data (surface source and downhole tool positions) and transit times, which were recorded in the seismic trace headers during the VSP acquisition, were attached as Appendix B without any modifications. The first column is the trace number. The second and third columns are the X (Easting) and Y (Northing) positions of each shot. The fourth column is the measured depth from the Kelly Bush (KB). The fifth and sixth columns are the arrival times of the seismic signal at the hydrophone and downhole geophone after the Maxis started the recording. The seventh column is the transit time between the hydrophone and geophone.

Table 1. Survey Parameters

Elevation of KB	26 m
Elevation of DF	26 m
Elevation of Sea Bottom	-395 m
Energy Source	150 cu in. G-gun fired at 120 bar
Source position	Navigation recorded in header
Source Depth	6 m below MSL
Reference Sensor	Hydrophone
Hydrophone Offset	Same as those of the sources
Hydrophone Depth	3 m below MSL
Tool Type	CSI
Tool Combination	Stand alone or dual
De-coupled Geophones	Yes
Shaker Fitted	Yes
Number of Axis	3
Geophone Type	SM-4 (gimballed)
Frequency Response	10-150 Hz
Sampling Rate	1.0 ms
Recording Time	5000 ms
Acquisition Unit	MAXIS
Recording Format	DLIS

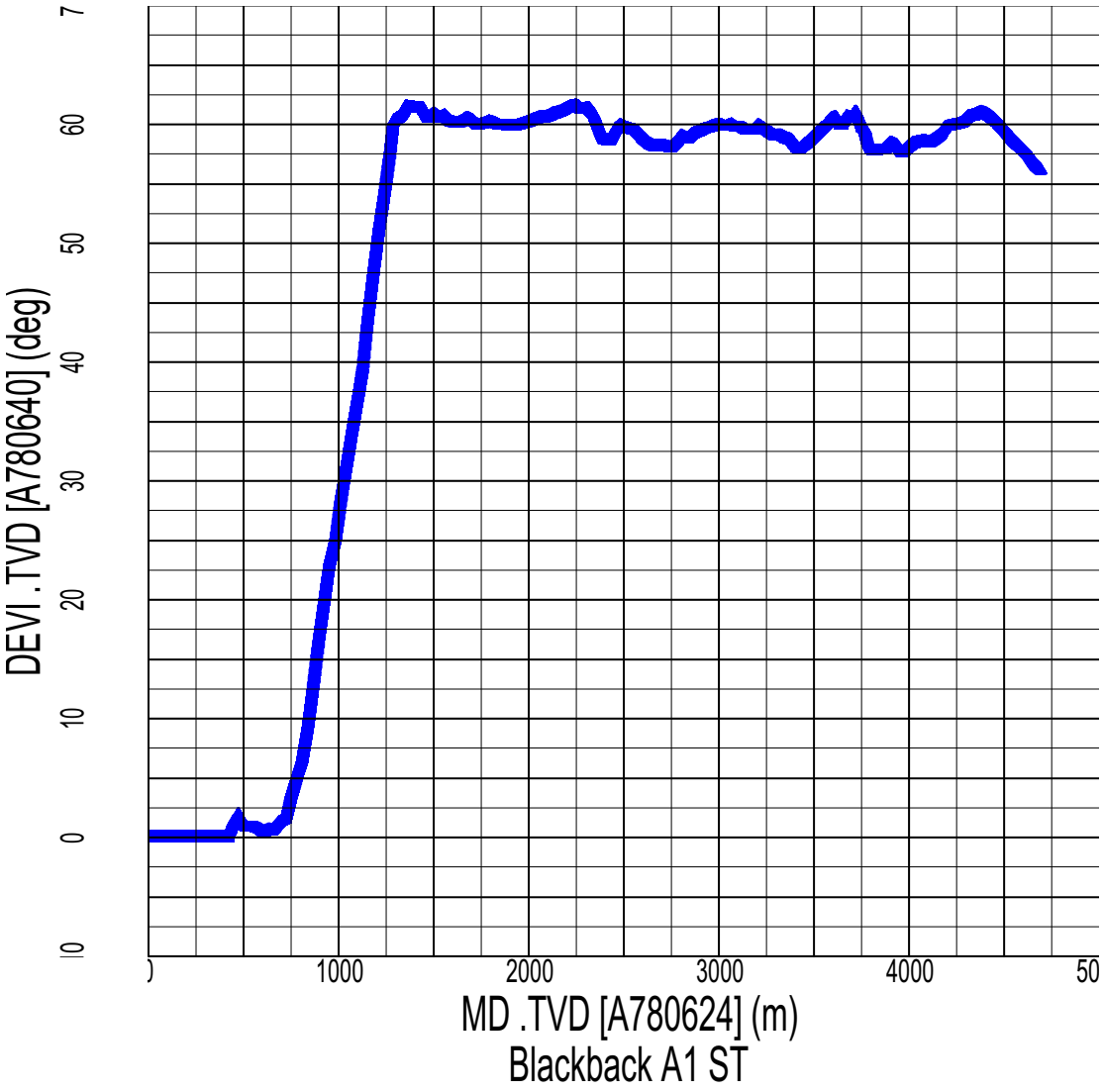

		# Points Total:	30808
Start Depth:	4694.99 m	**# Points Plotted:**	30808
Stop Depth:	0.00343438 m	**# Points Absent:**	0
Sampling Rate:	0.1524 m	**# Points Cut:**	0
X Max Value:	4694.84 m	**# > X Scale Max:**	0
X Min Value:	0 m	**# < X Scale Min:**	0
Y Max Value:	61.5898 deg	**# > Y Scale Max:**	0
Y Min Value:	0 deg	**# < Y Scale Min:**	0

Figure 1. Blackback A1 ST-1 well deviation

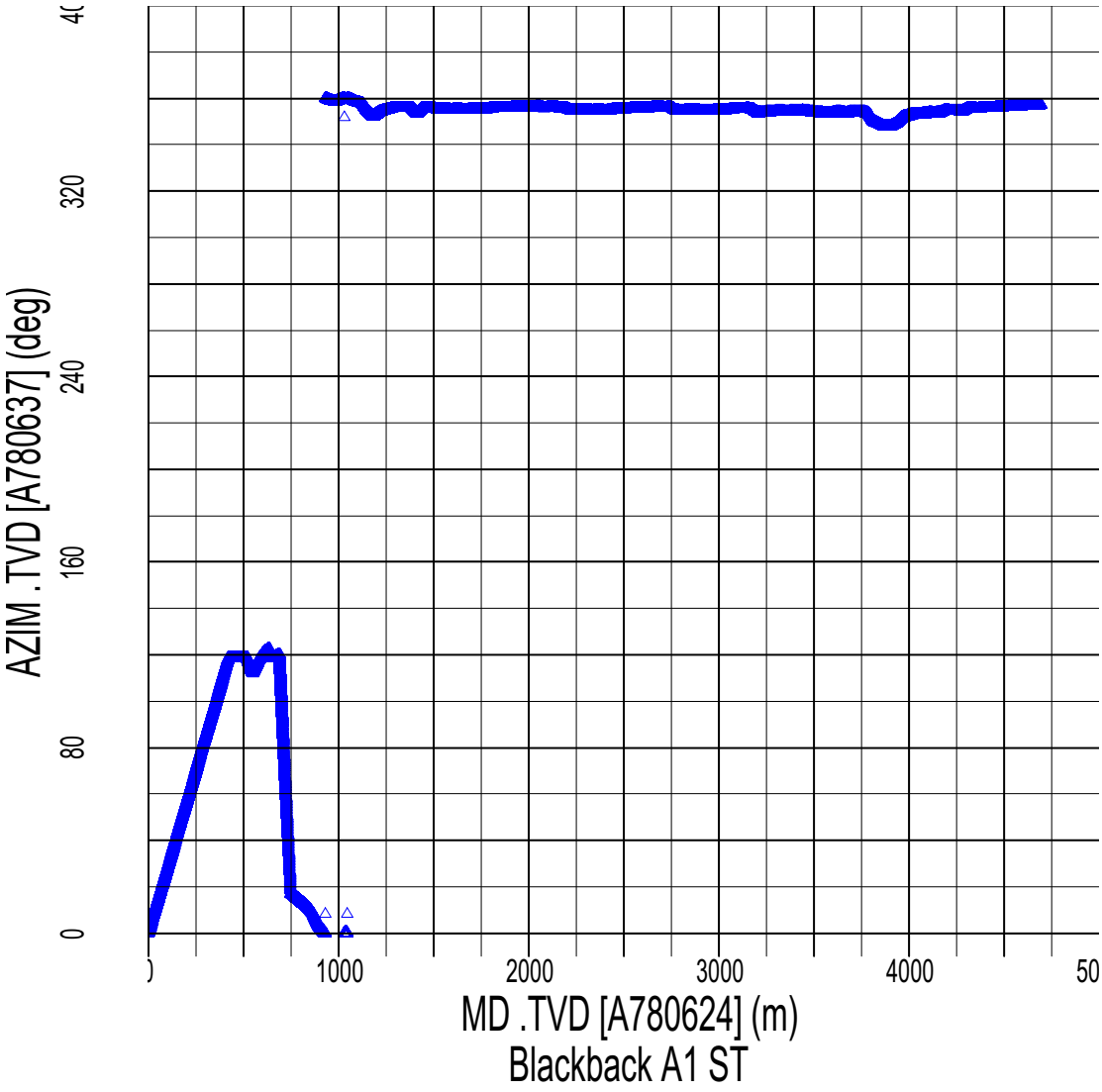

		# Points Total:	30808
Start Depth:	4694.99 m	**# Points Plotted:**	30808
Stop Depth:	0.00343438 m	**# Points Absent:**	0
Sampling Rate:	0.1524 m	**# Points Cut:**	0
X Max Value:	4694.84 m	**# > X Scale Max:**	0
X Min Value:	0 m	**# < X Scale Min:**	0
Y Max Value:	360 deg	**# > Y Scale Max:**	0
Y Min Value:	0 deg	**# < Y Scale Min:**	0

Figure 2. Blackback A1 ST-1 well azimuth

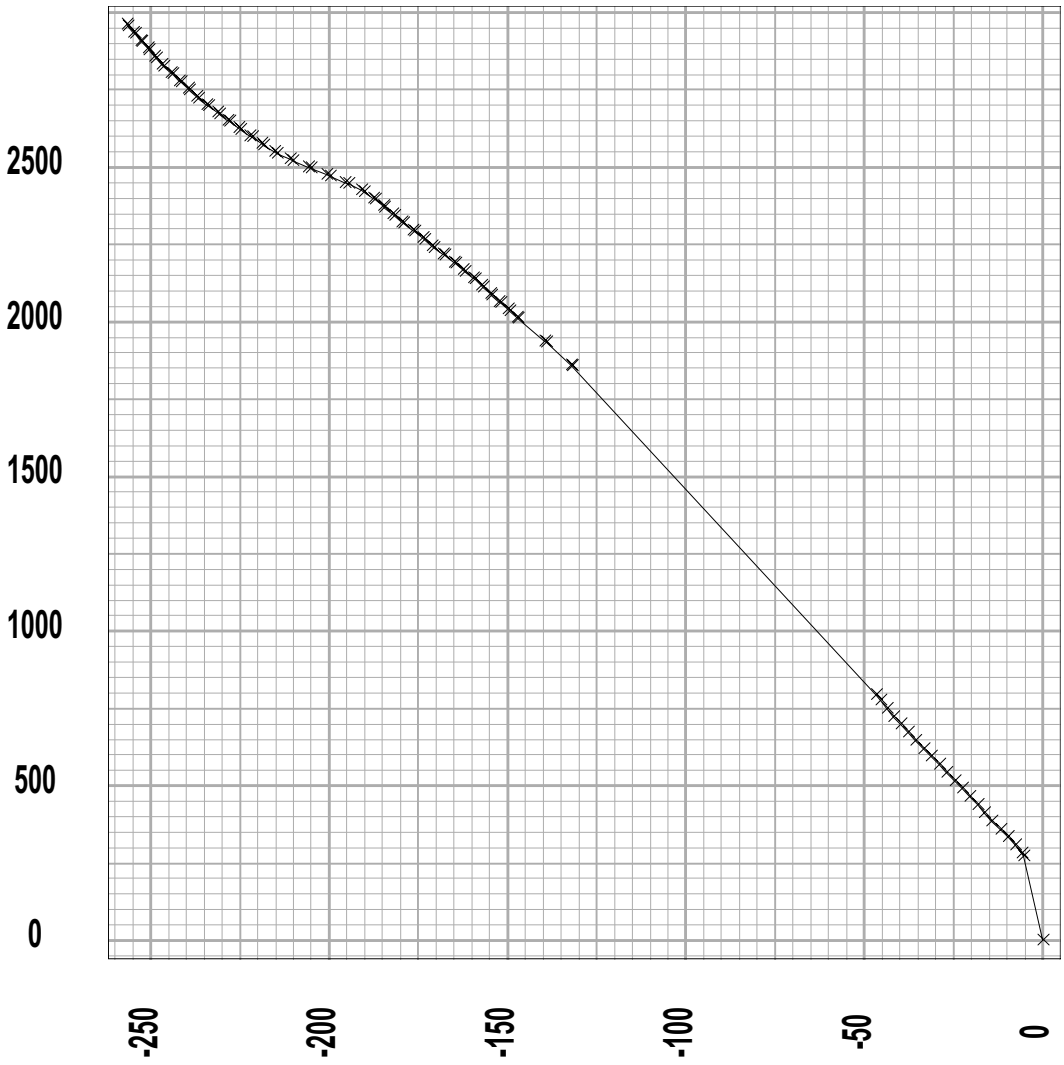

Figure 3. X-Y plane of geophone positions at Blackback A1 ST-1

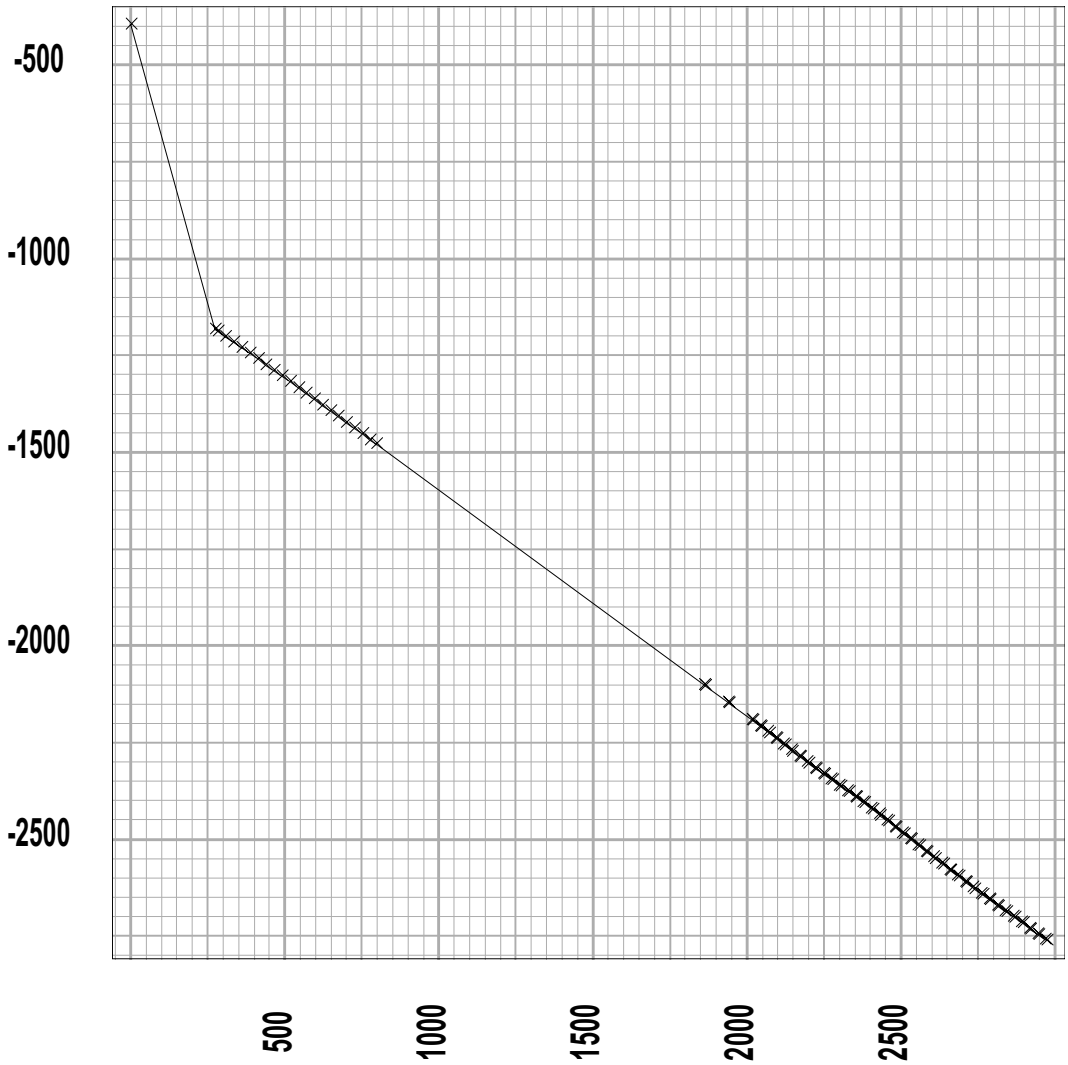

Figure 4. Sagittal (azimuthal) plane of geophone positions at Blackback A1 ST-1

2.3 Polarity Convention

An increase in acoustic impedance gives a positive reflection coefficient, is written to tape as a negative number and is displayed as a white trough under normal polarity. Polarity conventions are displayed in Figure 20.

3. Well Seismic Edit

The raw geophone/source position data and transit times of each shot are listed in Appendix B. By inspection, it is easy to note that there are some zeros in source positions and transit times. For the source positions, this means that the logging unit did not capture the navigation data or the navigation data were not sent to the logging unit at the appropriate time. For the whole survey, the dropout rate was very small, about 1 percent. For data processing, it was assumed that the missing source position would be the average of its sequentially neighboring shot positions. The edited navigation data were listed in Appendix C.

Both the geophone and hydrophone data were evaluated for signal/noise level and signature changes. Bad traces were identified and edited out. For example, the seismic data recorded at the measured depth of 4200 m were very noisy and this level was therefore deleted without further processing.

3.1 Data quality

The overall quality of the data was good. Note the following:

- **The Z component** was good on both Run-1 and Run-2. It is important to note that each source was approximately above the corresponding downhole geophones and the geophones were gimballed with their Z-components in the vertical direction. Thus, most of compressional energy at the first arrival was on the Z component.

  The first sea bottom multiple was clearly visible and might offer an opportunity of determining the water depth with their transit times. The shape of this multiple suggested that there was a channel in the well azimuthal direction. In the zone of Run-2, the multiple event reversed the normal trend (increasing time with increasing depth) and would be difficult to attenuate with velocity filtering. Fortunately, this event was out of the zone of interest.

- **The X and Y components** from Run-1 showed a fairly good S/N ratio, those from Run-2 had lower S/N ratio, especially on the Y component where the signal was weak.

  Some amount of the mode-converted downgoing shear energy can be clearly seen on both X and Y components. But these mode converted events were very weak in comparison to the compressional energy on Z component. By inspection of Figures 5A & B, it was noted that most mode conversions occurred at the sea bottom and the interface between BCHAN and MMIO formations. These mode converted shear events were recorded as downgoing events propagating at the shear velocity of the corresponding formation.

3.2 Transit Time Measurement

The transit time measured, Delta t, corresponds to the difference between first-break times recorded by surface reference and downhole sensors. The reference time (zero time) is the physical recording of the source signal by accelerometers on the gun or sensors positioned near the source. In this case, a hydrophone positioned 3.0 m above the gun was used as the reference. It is important that the actual recording starts before the signal arrives at the sensor. For the surface reference sensor, the recording starts immediately after the firing command was sent out from the Maxis. For the downhole sensor, the recording normally starts with a delay (blank time) after the firing command.

The blank time can be estimate by dividing the least source-receiver distance by the highest velocity along the ray path between the source and receivers.

All the first-break times were re-picked and the same first-break picking algorithm was used on both the hydrophone and the geophone channels. By comparing the raw data with the re-picked data, it was easy to note that there were some differences between them. All the differences were due to the nature of time picking in the field where minimal human interactions were involved. This was confirmed that some of the reference times in the raw data were at the start of recording.

The edited source position data and the re-picked transit times for both Run-1 and Run-2 were listed in Appendix C.

3.3 Correction to Datum

Seismic Reference Datum (SRD) used for VSP processing is at the mean sea level (MSL). The source was suspended 6.0 meters below MSL. A hydrophone was attached to the source 3.0 meters above the outlet ports and was used as the time reference. A static correction of 5.9 msec (OWT) would be applied to correct to SRD if the source is directly above the receiver. Otherwise, a geometry correction would also be applied. Indeed, both were applied simutaneously.

4. VSP Processing

The following subsections describe the main aspects of VSP processing schemes.

- stacking
- 3-component rotation
- up & down wavefield separation
- downgoing wave analysis
- predictive and waveshaping deconvolutions
- model building
- tomographic inversion
- Kirchhoff migration

4.1 Stacking

Several shots are normally fired for each downhole position. These multiple shot records offer an opportunity of increasing the signal-to-noise ratio. By stacking, the coherent signal would be enhanced whereas random noises would be suppressed. Here, the data were stacked using radio hydrophone channels as zero time reference. After stacking, break times were re-picked. As expected, most of them were very close to those shown on the field acquisition log print. An extra 3 msec was added to the one-way transit times to compensate for radio delay. Figure 5 shows the stacked data acquired at BBA1ST-1.

The re-picked transit times were corrected to true vertical times with SRD = MSL. Average velocity from SRD to the current receiver position and interval velocity between neighbouring receiver positions were then calculated. All the time and depth information was listed in Appendix D.

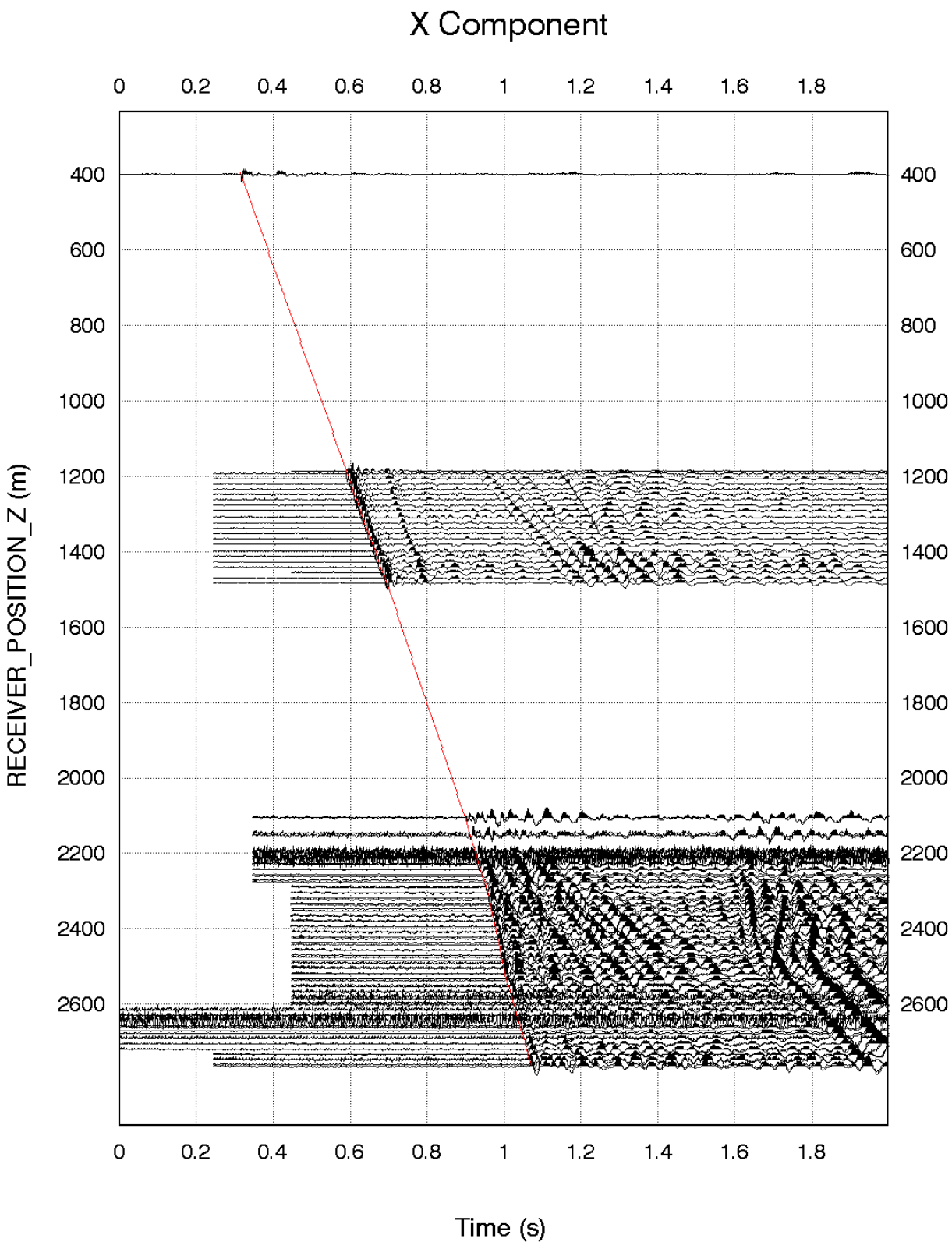

(A) Stacked X component

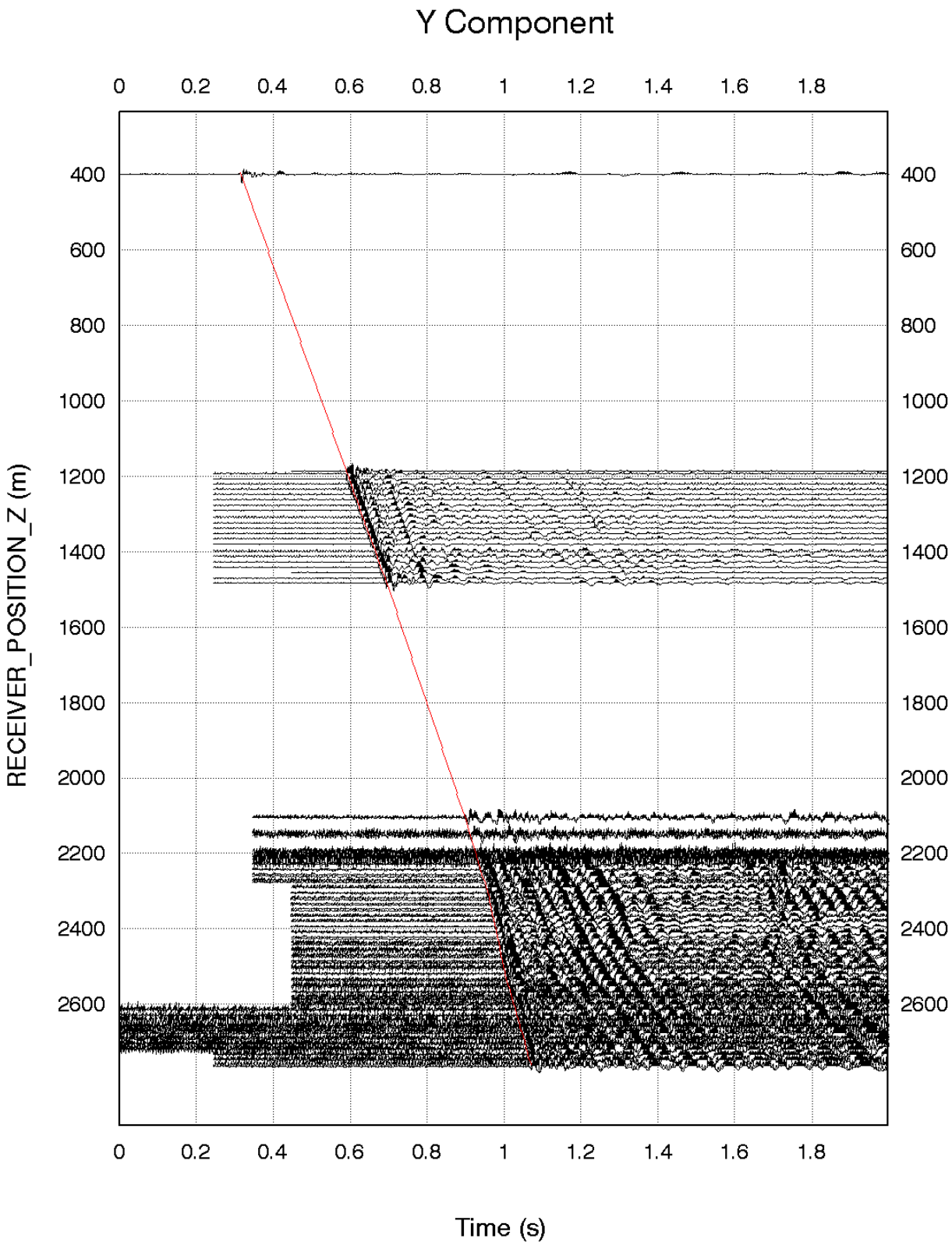

(B) Stacked Y component

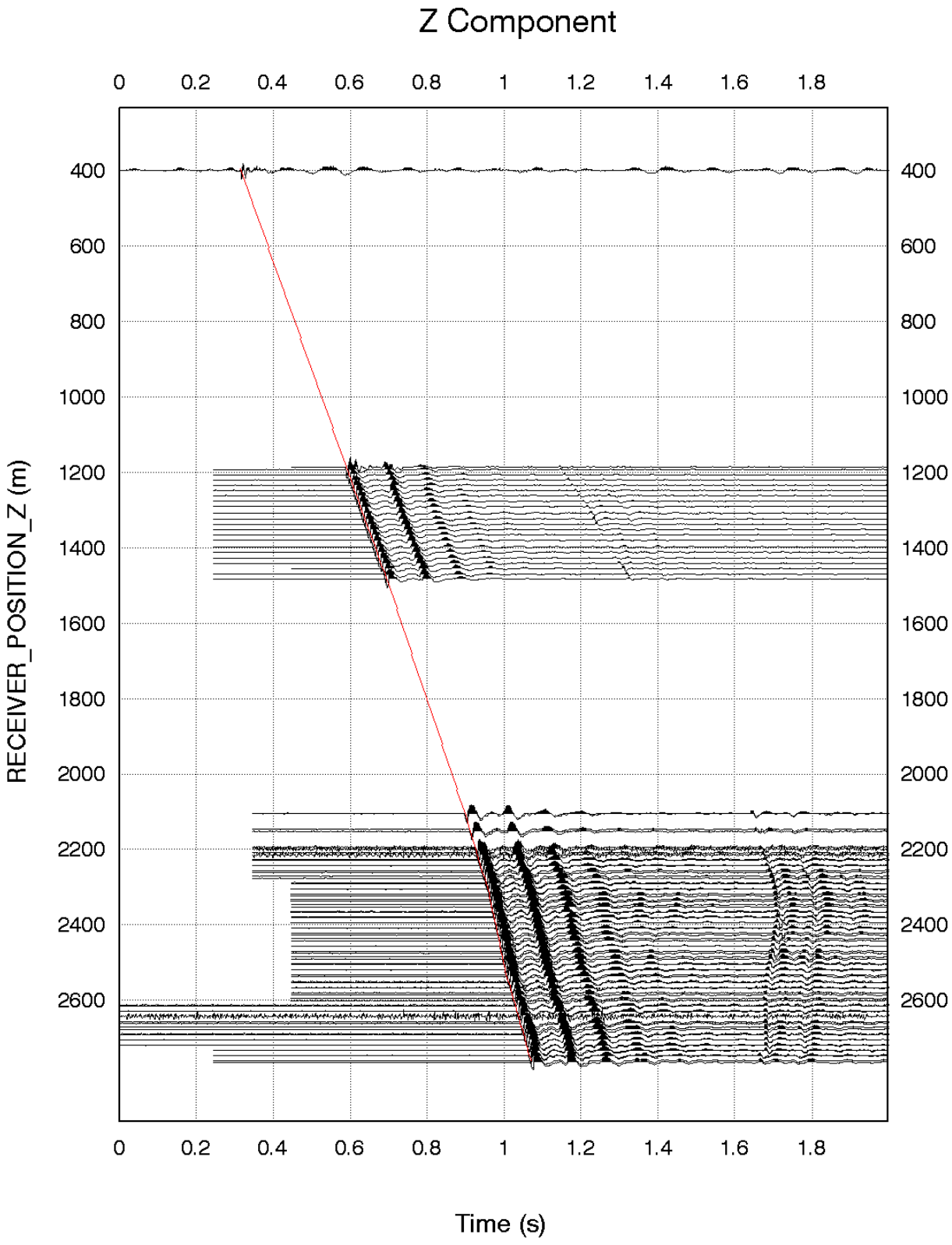

(C) Stacked Z component

Figure 5. Stacked sections of BBA1ST-1 seismic data.

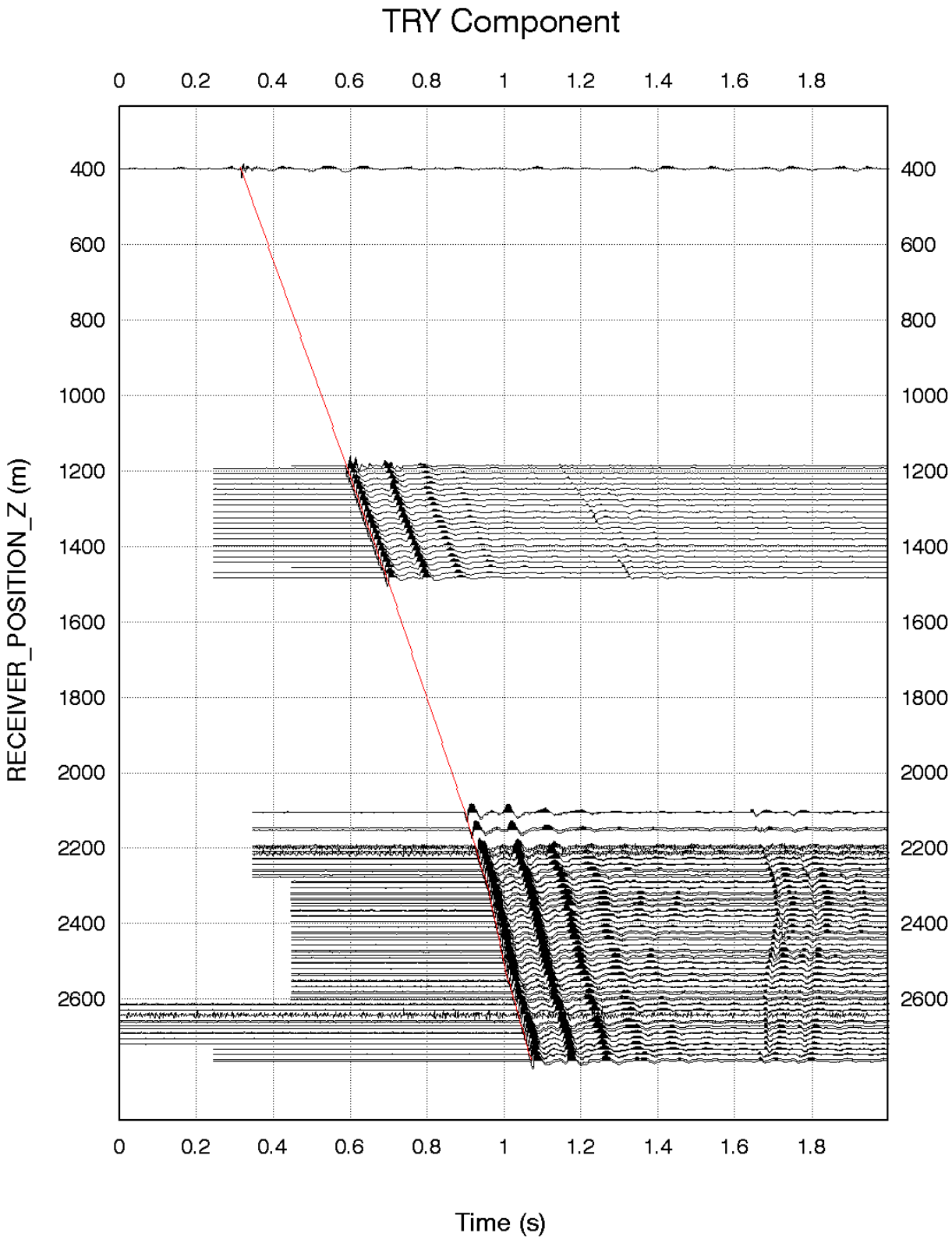

Figure 6. TRY component after 3-C rotation

4.2 3-C Rotation

Most source-receiver configurations were very close to vertical and the primary arrival (compressional wave) were mainly on the Z component. Indeed, the Z components were more than five times greater than the horizontal components at most levels. For improved VSP processing, a three-component rotation was applied. After opening a narrow time window (60 msec.) around the first arrival, a rotational vector was first applied on two components (X and Y) in the direction of maximum horizontal energy (HMX) to obtain HMX and HMN. Then, another rotational vector was applied on two components (HMX and Z) in the direction of maximum downgoing energy (TRY) to obtain TRY and NRY. This was computed for each geophone position. The main benefit of computing the TRY component is to have most compressional energy at the first arrival concentrated along one component (TRY) and rotate out downgoing shear energy (Figure 6).

Definitions for three component rotation

HMX projection (**H**orizontal **M**a**X**imum) The projection of the X and Y components into the direction of maximum horizontal compressional energy.

HMN projection. (**H**orizontal **M**i**N**imum) The projection of the X and Y components into the direction of minimum horizontal compressional energy. The Z, HMX and HMN form an orthogonal data set.

TRY projection (**T**angent to direct **R**a**Y**) The projection Z and HMX into the direction maximum downgoing compressional energy

NRY projection (**N**ormal to direct **R**a**Y**) The projection Z and HMX into the direction minimum downgoing compressional energy. The NRY and TRY are perpendicular to each other and the NRY, TRY and HMN form a second orthogonal data set.

4.3 Velocity filter

The TRY downgoing coherent energy was estimated using nine (9) levels median velocity filter. The filter array was moved down one level after each computation and the process was repeated level by level over the entire dataset.

The residual wavefield was obtained by subtracting the downgoing compressional wavefield from the total wavefield. The residual wavefield was dominated by reflected compressional events.

The TRY upgoing wavefield was enhanced by making a median stack of the upgoing aligned traces using a seven (7) levels median filter.

Table 2. Median velocity filter parameters

Internal normalisation window	500 ms
No of levels to estimate downgoing P	9
No of levels to enhance upgoing P	7

4.4 Downgoing wave analysis

Power spectrum of TRY component for entire interval is presented in Figure 7. In general, the frequency band narrows as the distance between the source and receiver increases mainly due to anelastic attenuation. At the sea bottom, the power spectrum can reach up to 120 Hz. At 1200 m, the high end of the spectrum drops to about 80 Hz and at 2500 m, this further drops to 65 Hz.

The effects of air bubble from the gun on the power spectrum are clearly visible. The oscillating variation of the power spectrum is due to the constructive and destructive interference of the bubble and primary signals.

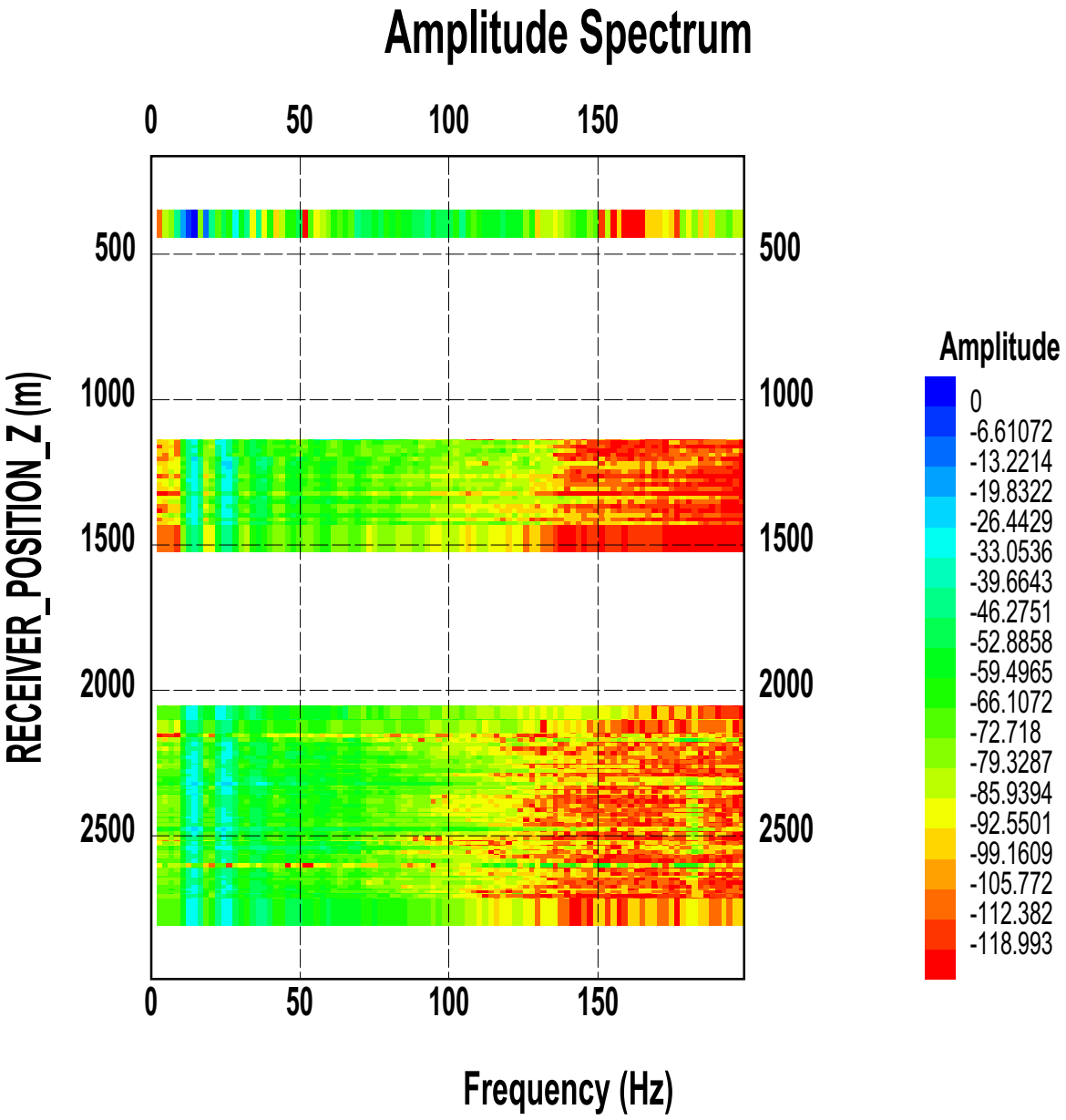

Figure 7. 2D power spectrum on Z component indexed in MD (meters)

Both maximum and minimum amplitudes of the downgoing wave are shown in Figure 8. Theoretical decay curves are computed and displayed together with the observed amplitudes. The theoretical curve is based on the following equation:

$$AMP = B_0 (t^{-(1+\alpha)}) \exp(-\beta t) \qquad (1)$$

Equation (1) is the true amplitude recovery (TAR) function used in VSP processing where alpha and beta are the spherical divergence and attenuation factors. Two sets of parameters were used for the analysis. The first set was $\alpha = 1.3$ and $\beta = 0.1$ (shown as AMP-1 in Figure 8) and the second set was $\alpha = 1.3$ and $\beta = 0.5$ (shown as AMP-2).

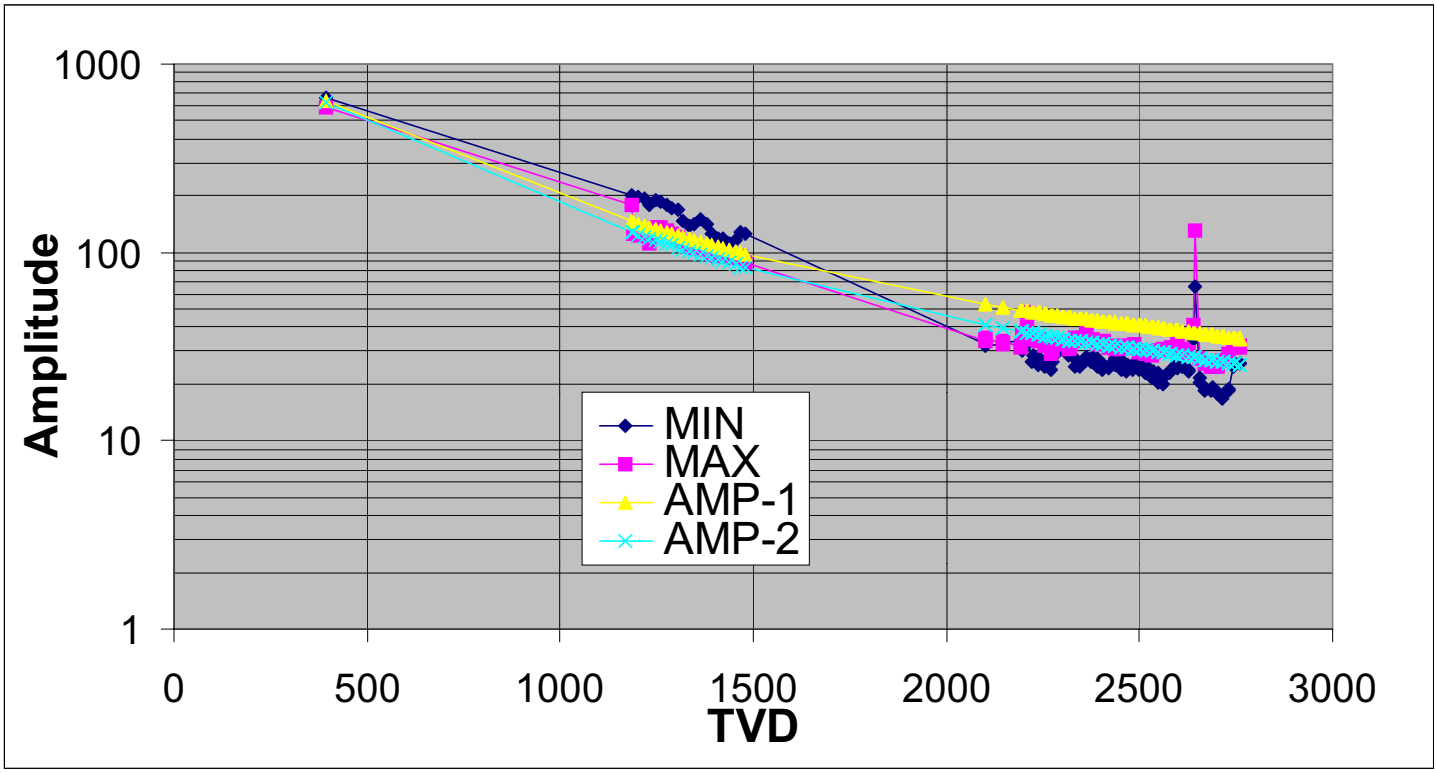

Figure 8. VSP amplitude analysis

Amplitude analysis shows that the amplitude decay in depth less than 1500 m is much less than that in depth greater than 1500. This variation in amplitude attenuation can be attributed to two major factors. The first one is the transmission loss due to the existence of large acoustic impedance contrasts between 1500 and 2000 m. The other is the variation of anelastic attenuation, i.e. the formations in the shallow section (< 1500m) are less attenuative than those in the deep section (> 1500 m).

4.5 Predictive and waveshaping deconvolution

The predictive deconvolution uses information from the earlier part of a seismic trace to predict and deconvolve the latter part of that trace. Some types of systematic noise, such as reverberations and multiples can be predicted. The predictive deconvolution operator is designed trace by trace based on the downgoing wavefield, opening 20 ms before the first break with a window length of 2500 ms.

The prediction time is chosen to be 60 ms. Once the design is made upon the downgoing wavefield, it is applied to the downgoing and upgoing wavefield at the same level.

The waveshaping deconvolution operator is a double sided operator and is designed trace by trace opening 20 ms before the first break with a window length of 2500 ms. The desired output is chosen to be the truncated version of the auto-correlation function of the down-going wavefield after the predictive deconvolution. The truncation point is chosen to be at the third zero crossing of the auto-correlation function. Again, once the design is made upon the downgoing wavefield, it is applied to the downgoing and upgoing wavefield at the same level.

The trace by trace deconvolution is applied in order to collapse the multiple sequence in both the down- and up-going wavefields. For a VSP in a layered model, both the down- and up-going wavefield should have very similar characteristics. If a deconvolution operator can suppress the down-going wave sequence, it should also be able to suppress the up-going wave sequence in the same way. However, if the up-going wave is significantly different from the down-going wave, the deconvolution would become less effective.

The results of predictive and waveshaping deconvolutions show that the suppression of the multiple sequence was completely successful on the down-going wavefield (Figures 9E&G and Figures 10 E&G), but was less impressive on the up-going wavefield. This was mainly due to variations in character between the down and up going wavefields. Also note that both down and up going wavefields may contain mode converted shear and diffractions, these noises are comparable in magnitude to the reflected up-going wavefield, but they are negligible in comparison to the primary down-going wavefield.

Table 3. Predictive and waveshaping deconvolution parameters

Predictive	
Opening	ms before first-break
Operator length	2500 ms
Autocorrelation length	1250 ms
Prediction time	60 ms
Noise level	1 %
Waveshaping	
Operator length	2500 ms
Noise level	1 %
Output wavelet	Auto-correlation at 3rd zero crossing
Wavelet delay	1250 ms

Figure 9 shows the results of each processing step for Run-1. Figure 9A is the VSP section after bandpass filtering and muting at BBA1ST-1.

Figure 9B is the downgoing wavefield after applying a median velocity filter to the VSP section shown in (A).

Figure 9C shows the residual wavefield obtained by subtracting the down-going wavefield (B) from the total wavefield (A). Coherent up-going events can be clearly seen, but there are some significant down-going events.

Figure 9D is the enhanced upgoing wavefield obtained by applying a median velocity filter to the residual wavefield (C). Downgoing events in the residual wavefield have been filtered out.

Figure 9E shows the result of predictive deconvolution of the downgoing wavefield (B). For each trace, an independent deconvolution operator was designed and applied. The predictive deconvolution filter has been able to suppress the multiple sequences of the down-going wavetrain (B) into a simple wavelet (E).

Figure 9F displays the upgoing wavefield after predictive deconvolution. At each depth level, the corresponding predictive deconvolution operator applied to the downgoing wavefield in (E) was used.

Figure 9G displays the result of the waveshaping deconvolution of the downgoing wavefield (E). At each depth level, the desired output was chosen to be the truncated version of the auto-correlation function. The truncation was made at the third zero crossing of the auto-correlation function.

Figure 9H shows the result of the waveshaping deconvolution of the upgoing wavefield. For each trace, the corresponding waveshaping deconvolution operator applied to the down-going wavefield in (G) was used.

The same processing sequences were applied to Run-2 and Figure 10 shows the result of each corresponding step.

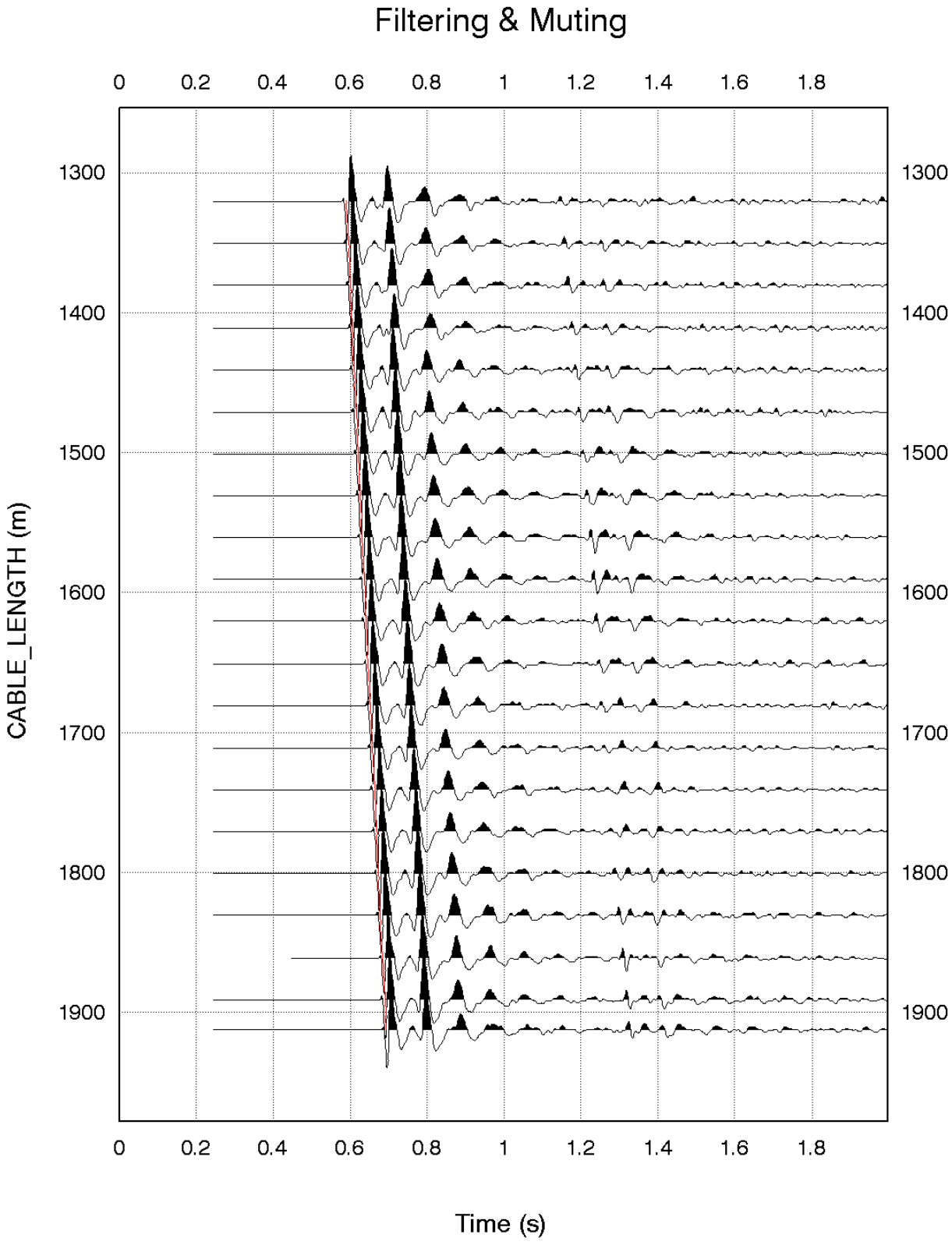

(A) Seismic data after bandpass filtering and muting of Run-1at Blackback A1 ST-1

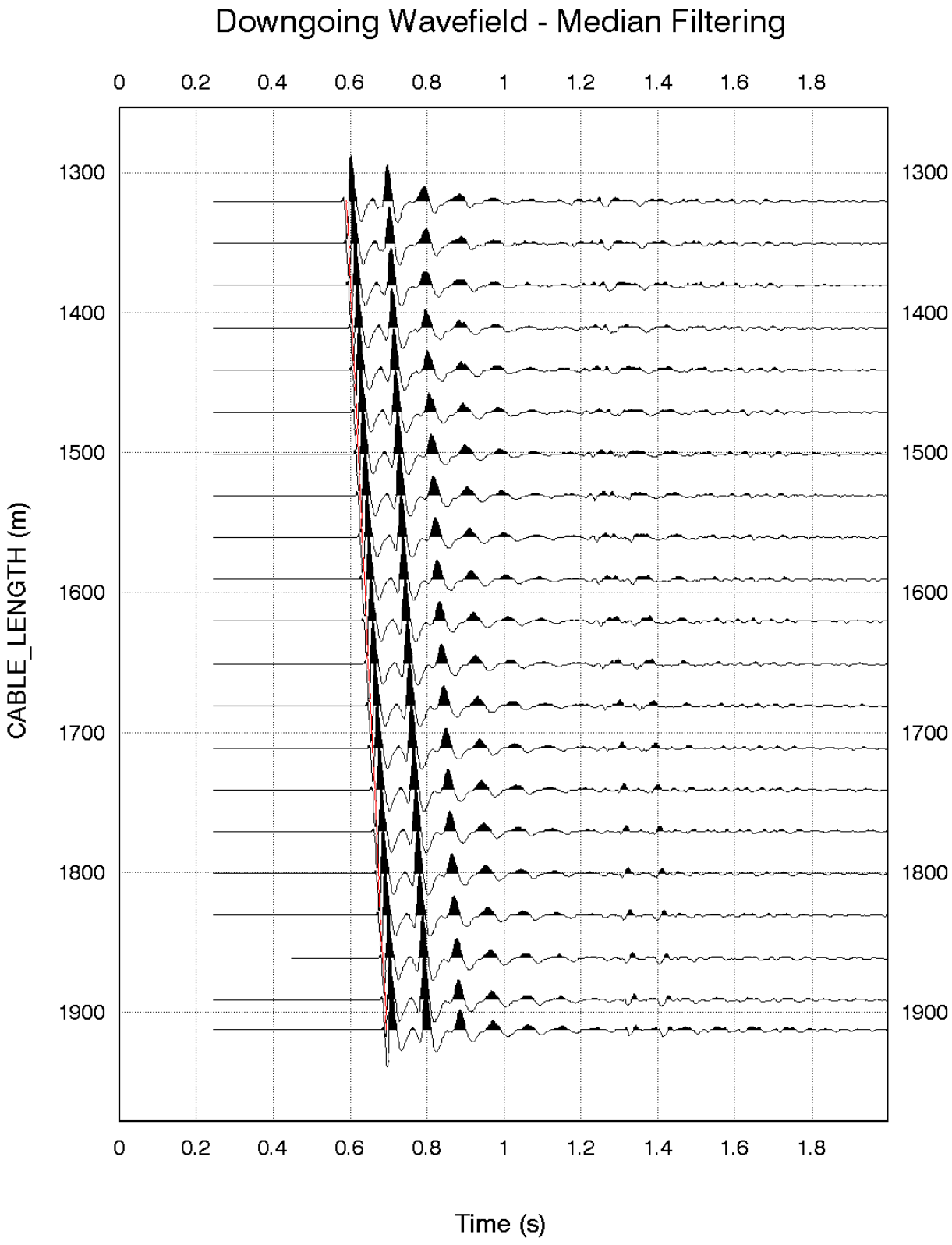

(B) Downgoing P wave after velocity filtering

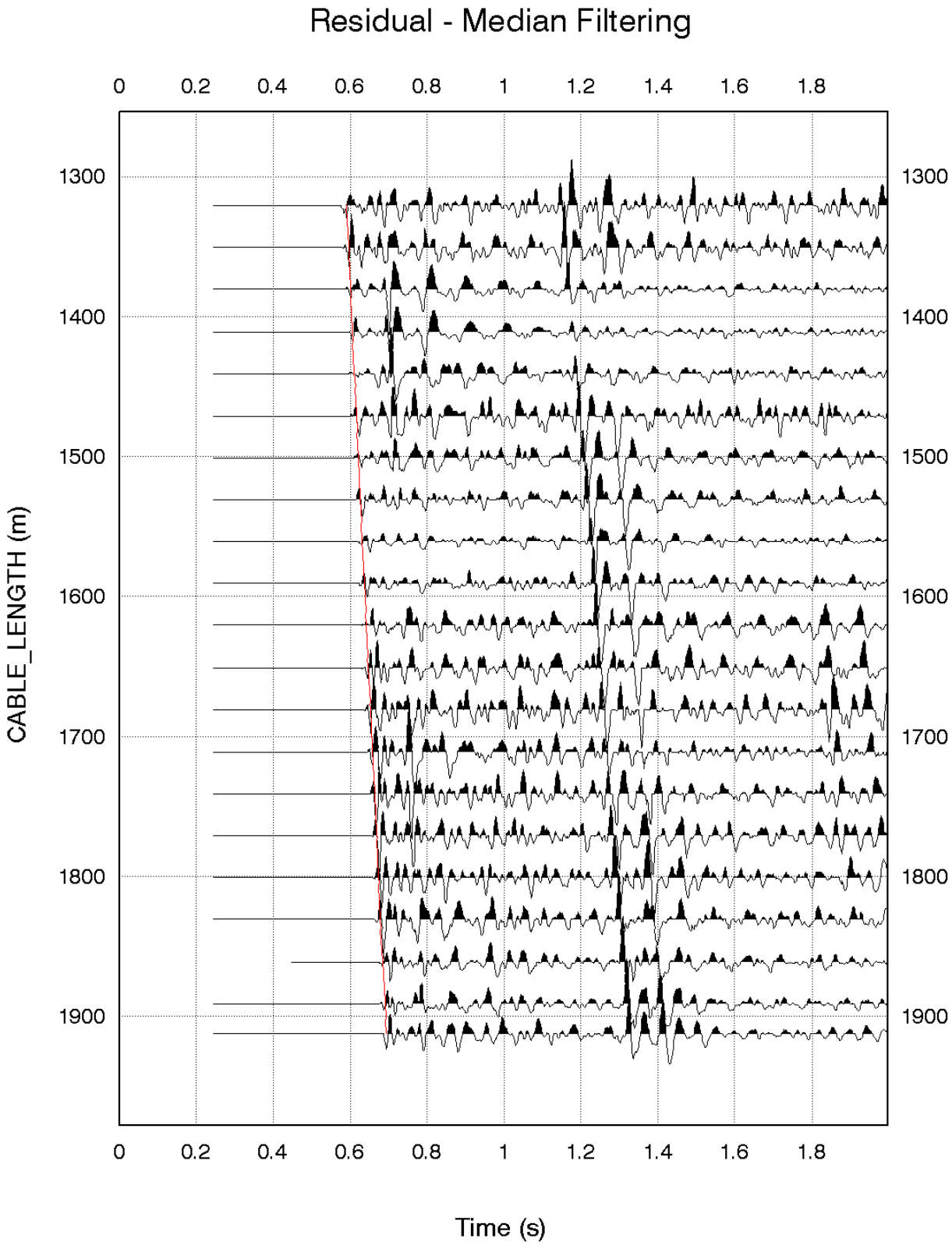

(C) Residual wavefield after median velocity filtering

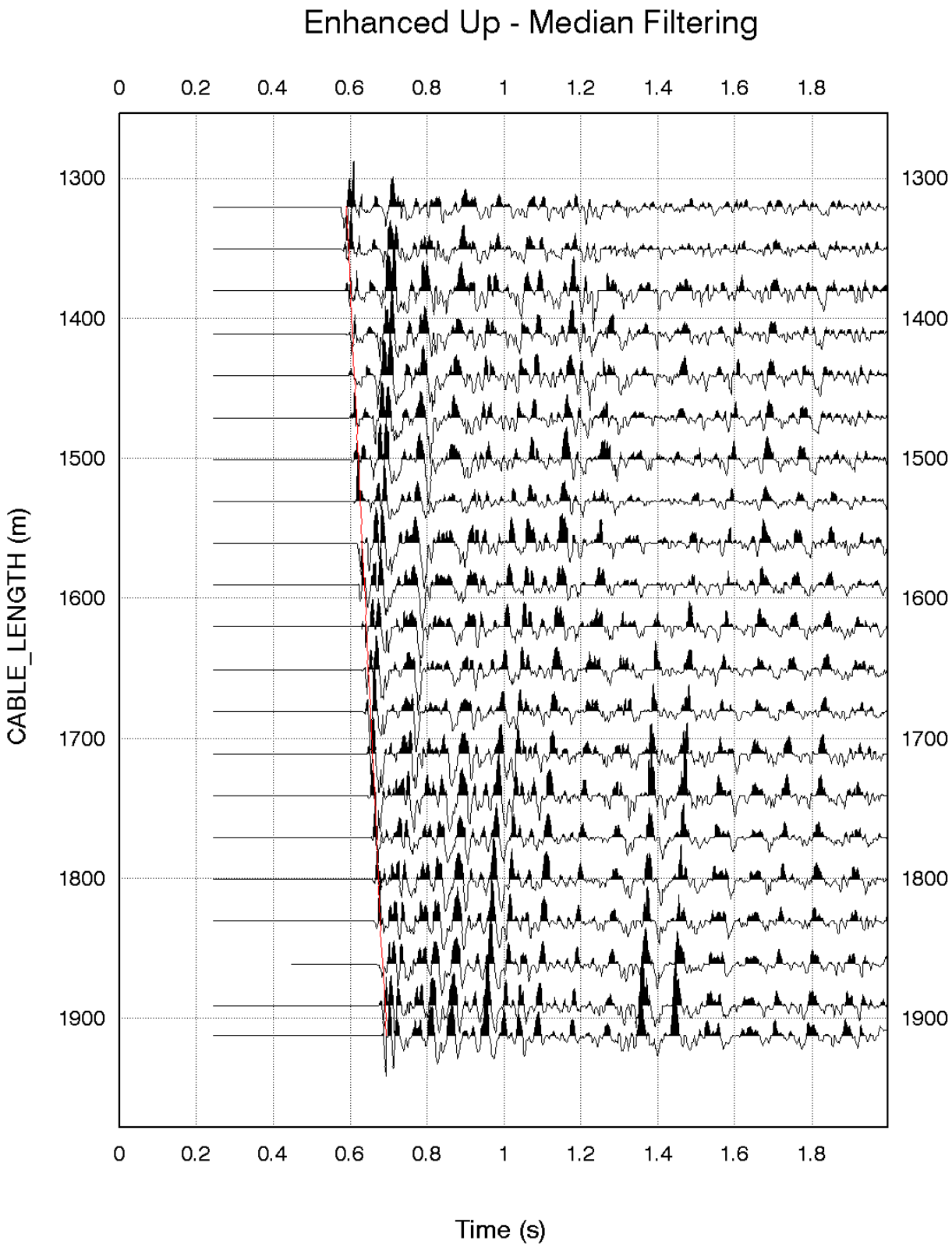

(D) Enhanced Upgoing P after applying a median velocity filter to the residual wavefield

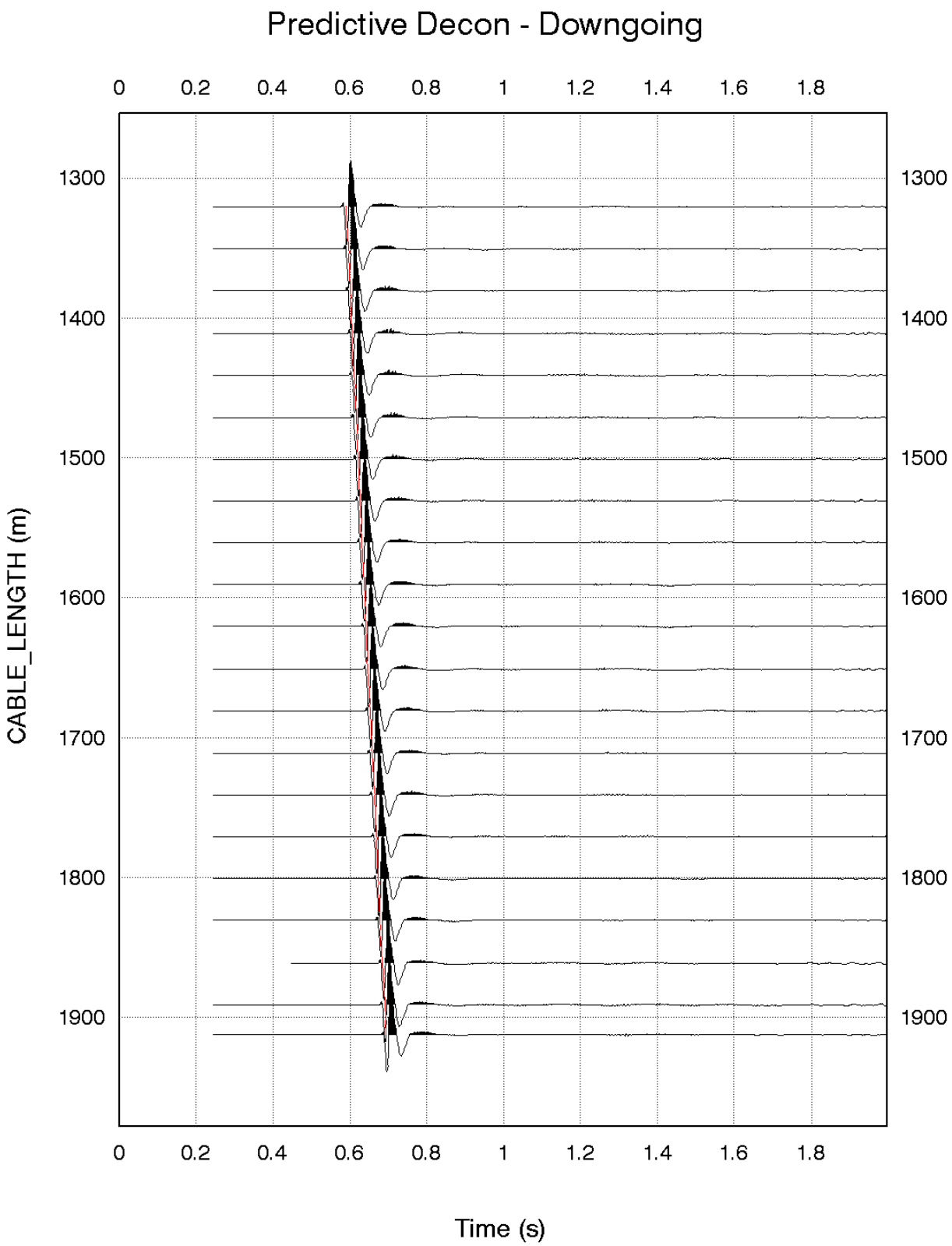

(E) Downgoing P after predictive deconvolution

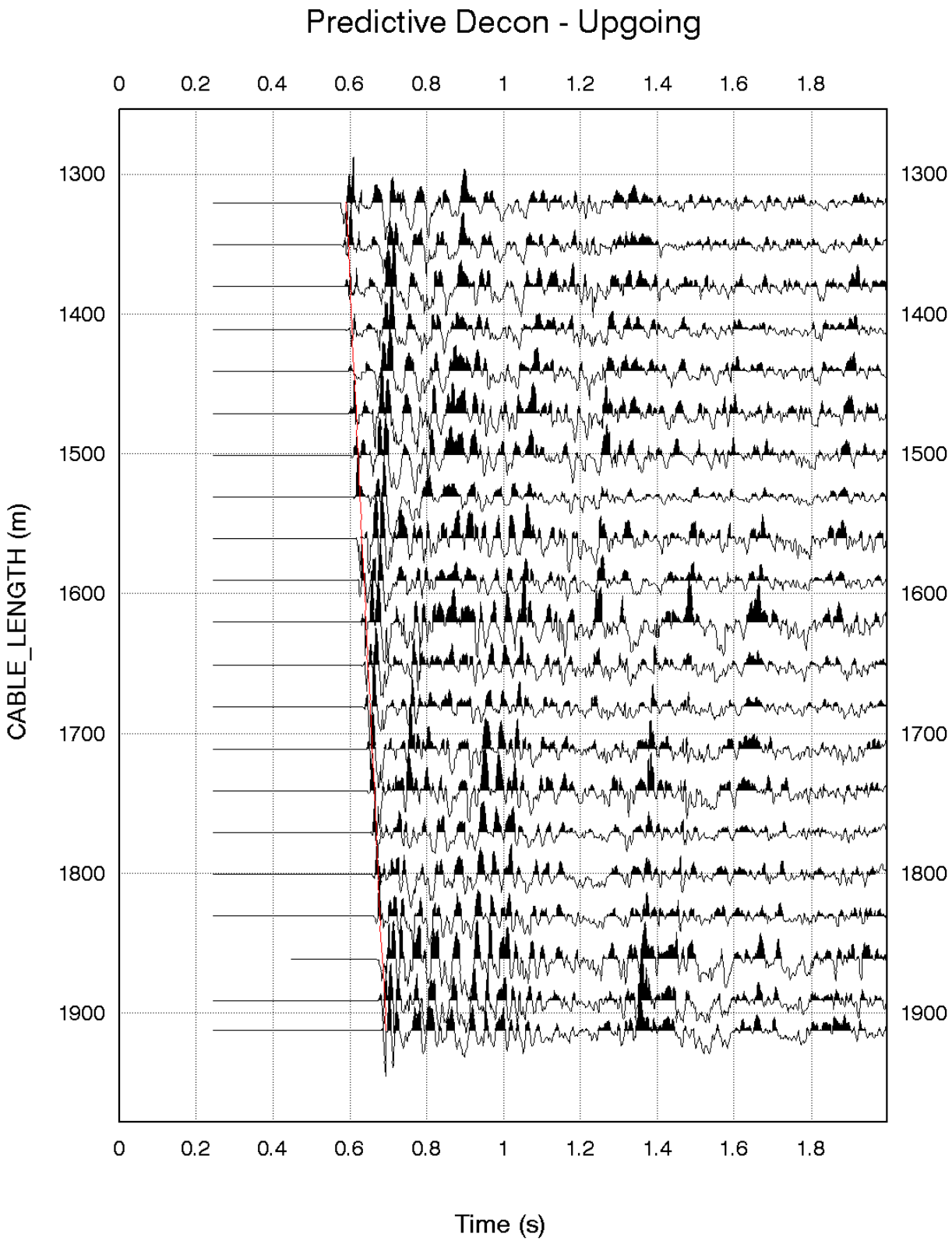

(F) Upgoing wavefield after predictive deconvolution

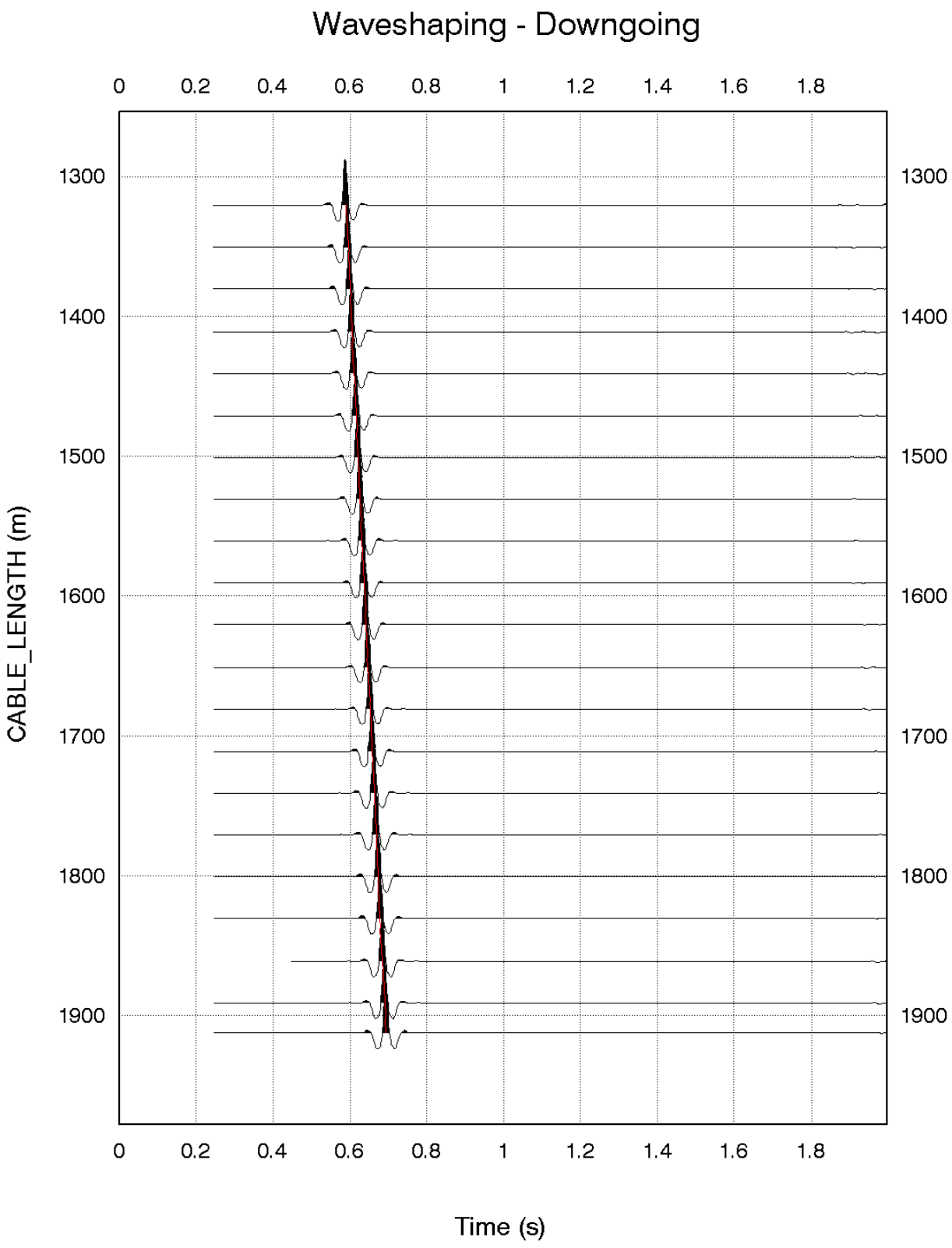

(G) Downgoing wavefield after waveshaping deconvolution

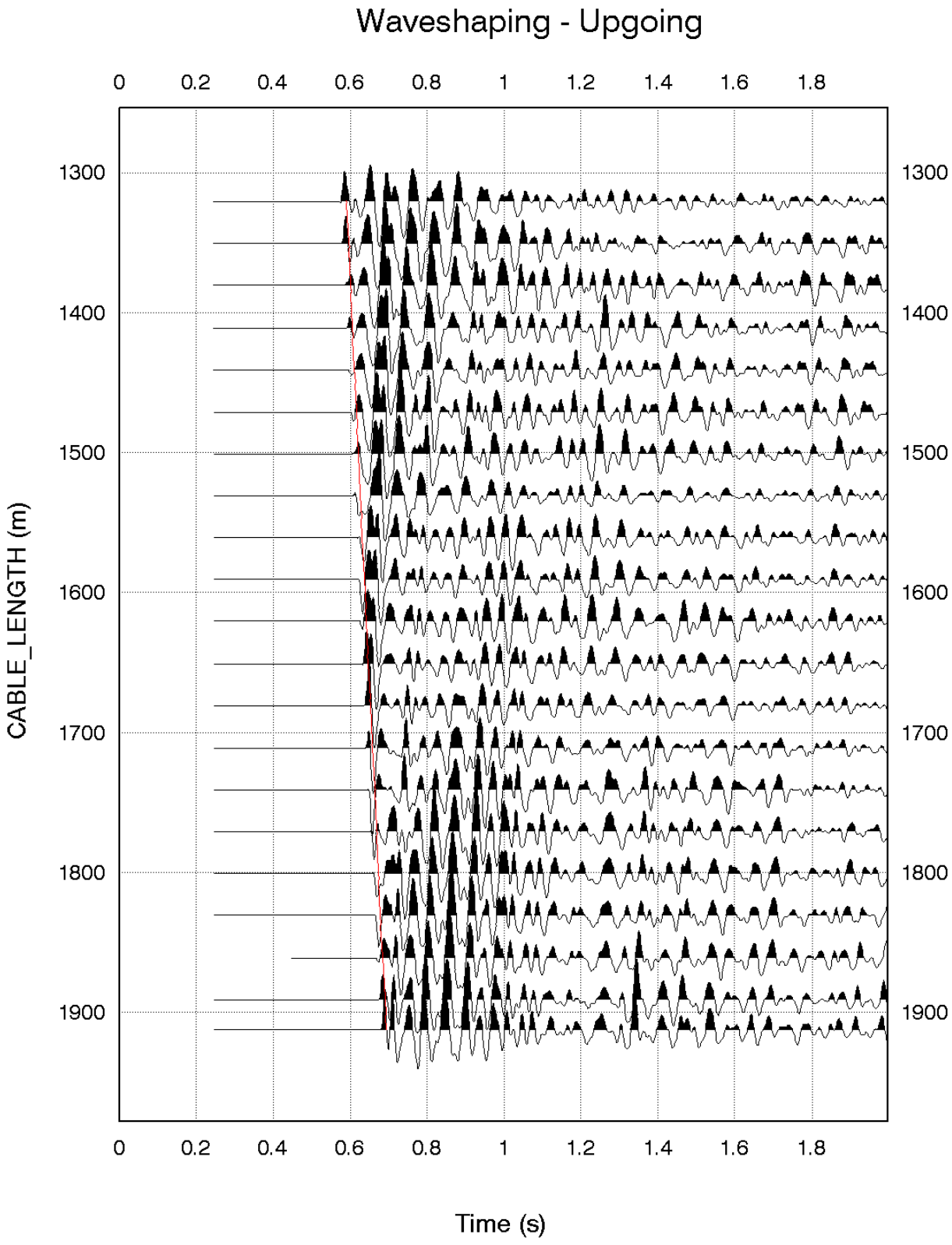

(H) Upgoing wavefield after waveshaping deconvolution

Figure 9. Results of each processing steps for Run-1

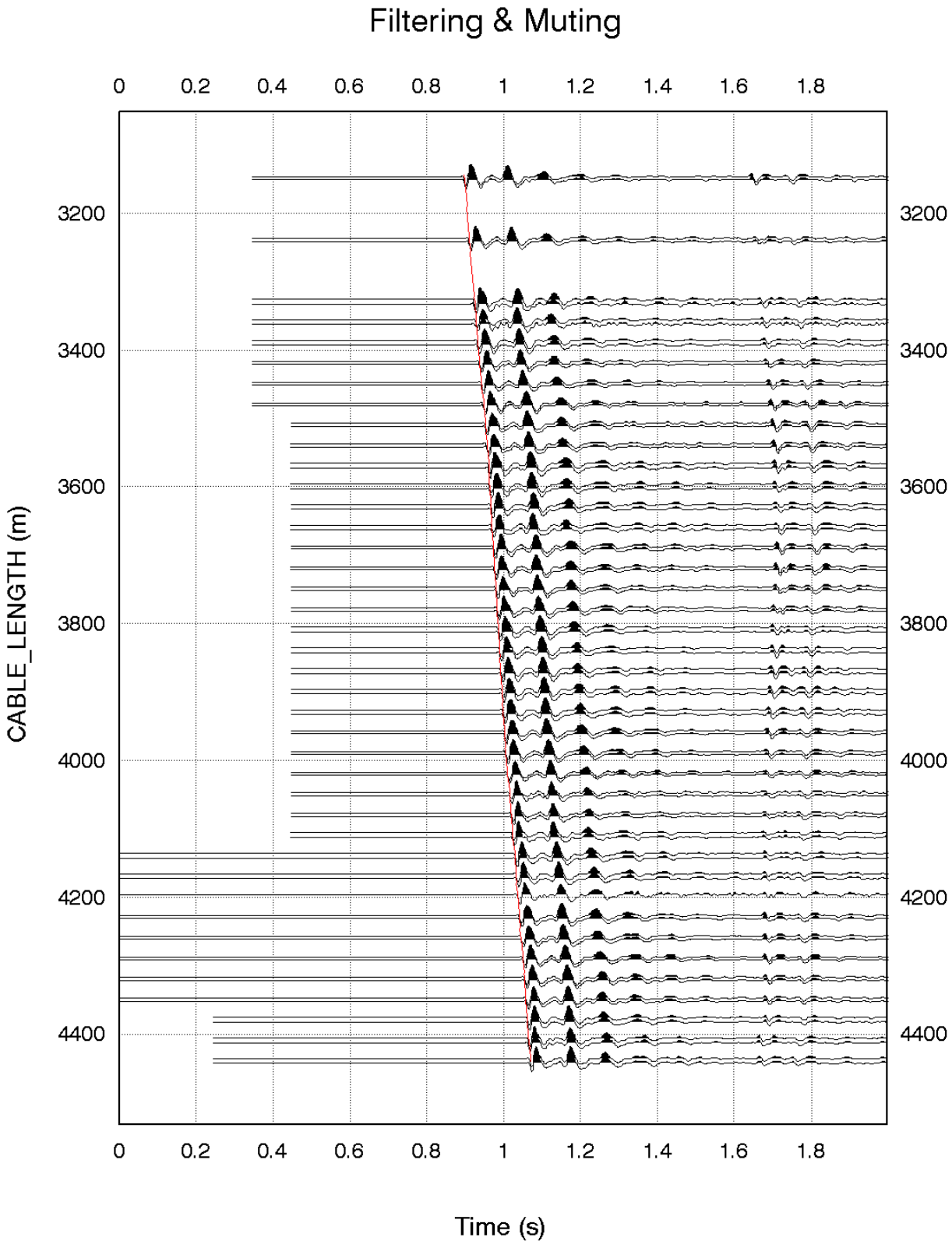

(A) Seismic data after bandpass filtering and muting of Run-2 at Blackback A1 ST-1

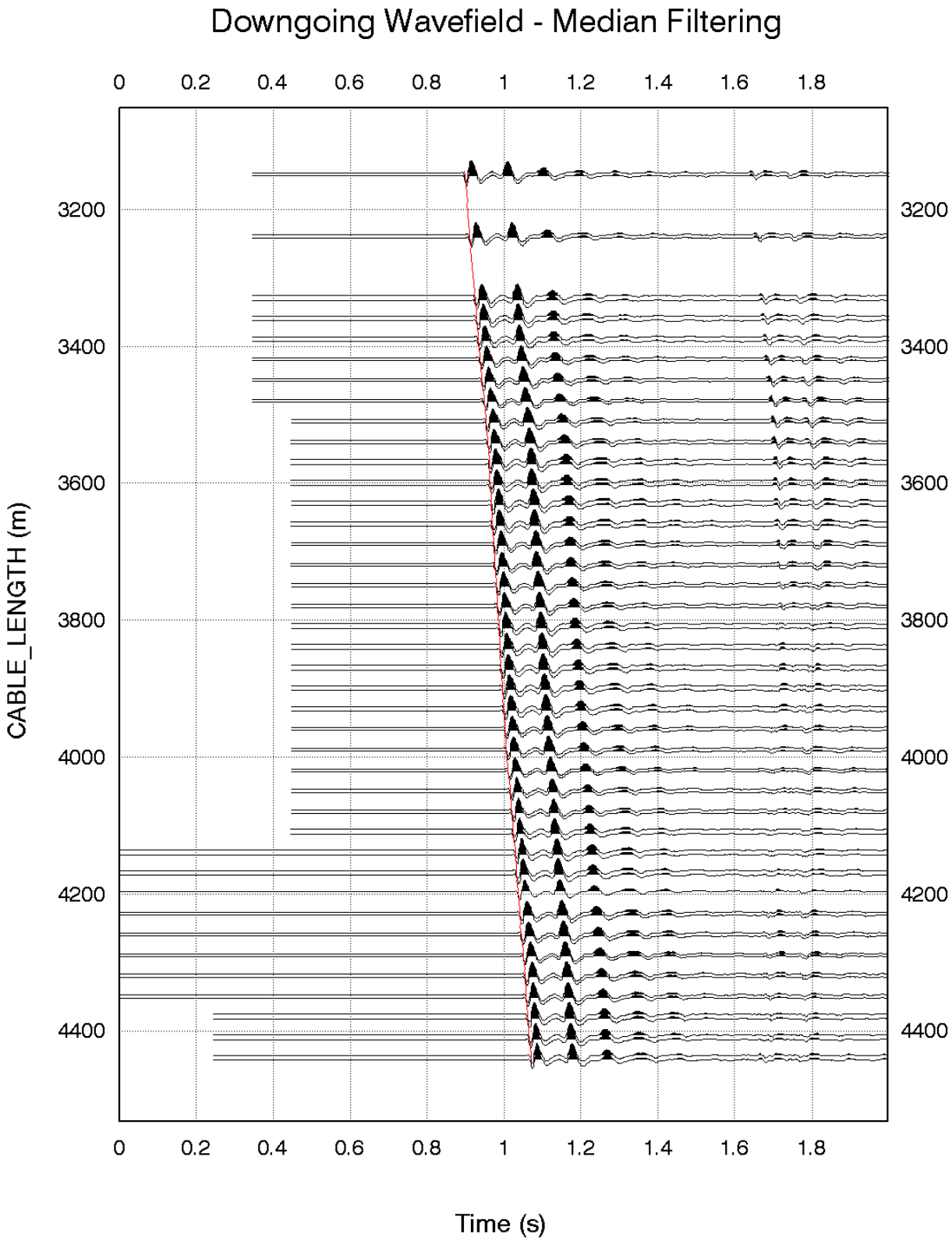

(B) Downgoing wavefield wave after velocity filtering

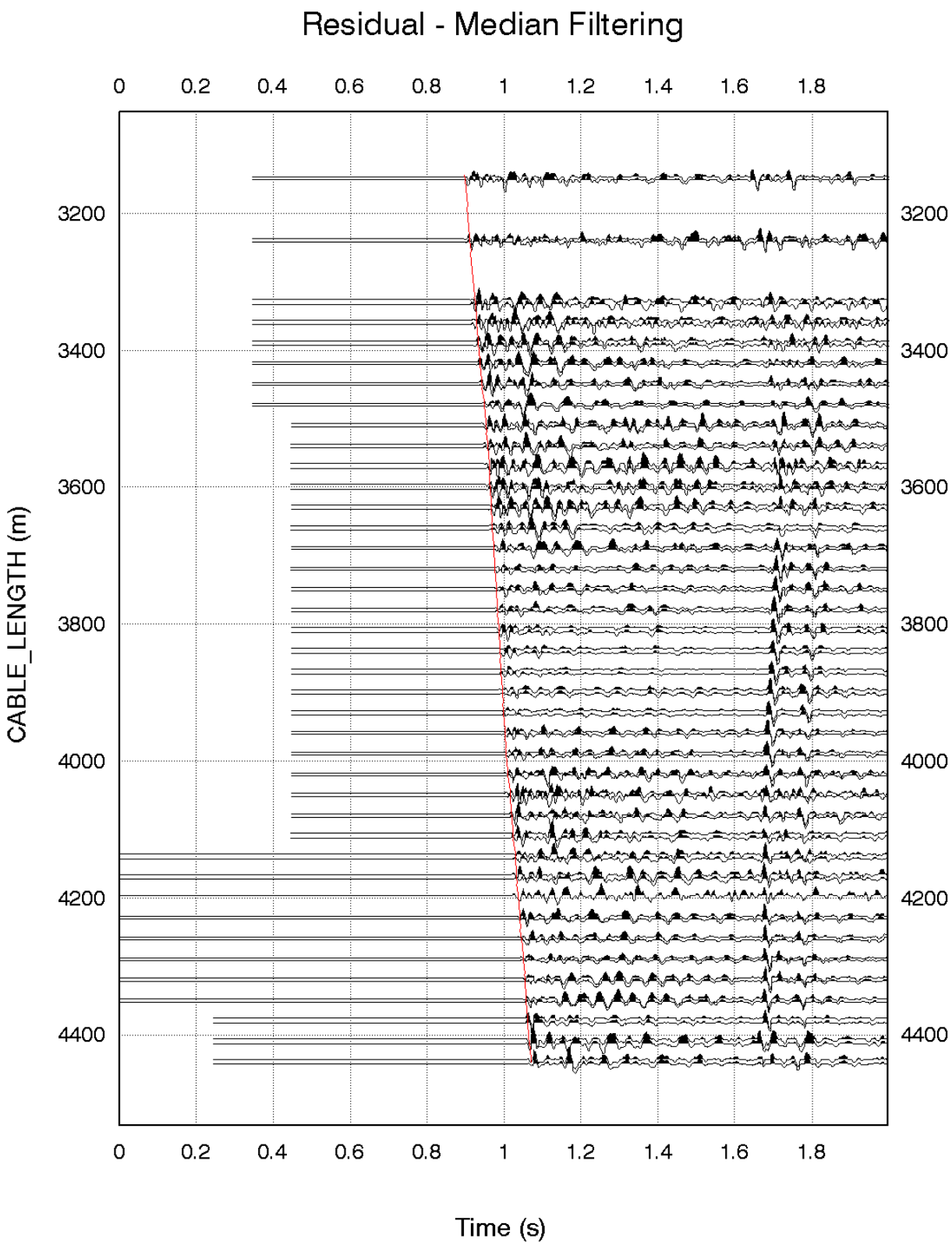

(C) Residual wavefield after median velocity filtering

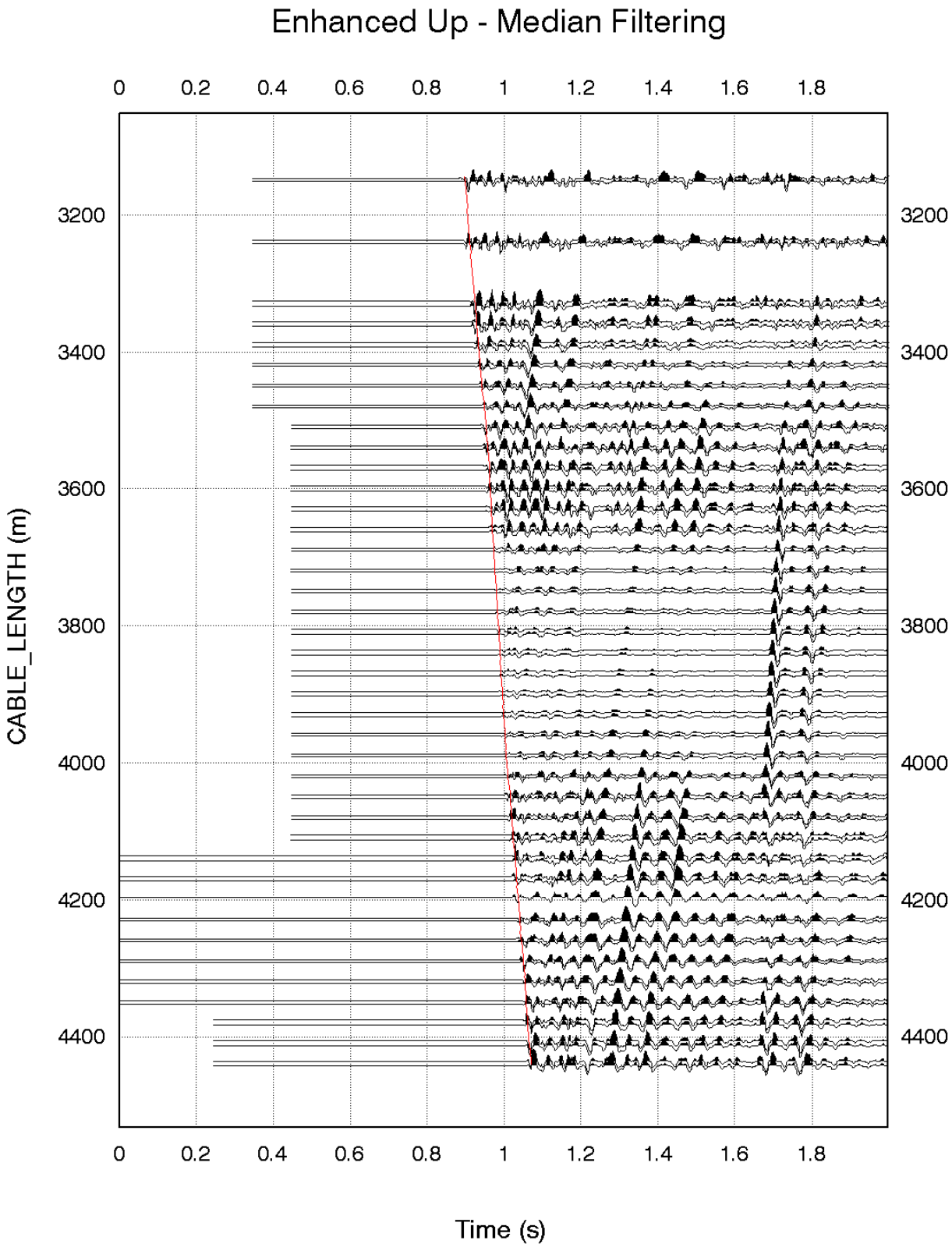

(D) Enhanced upgoing wavefield after applying a median velocity filter to the residual wavefield

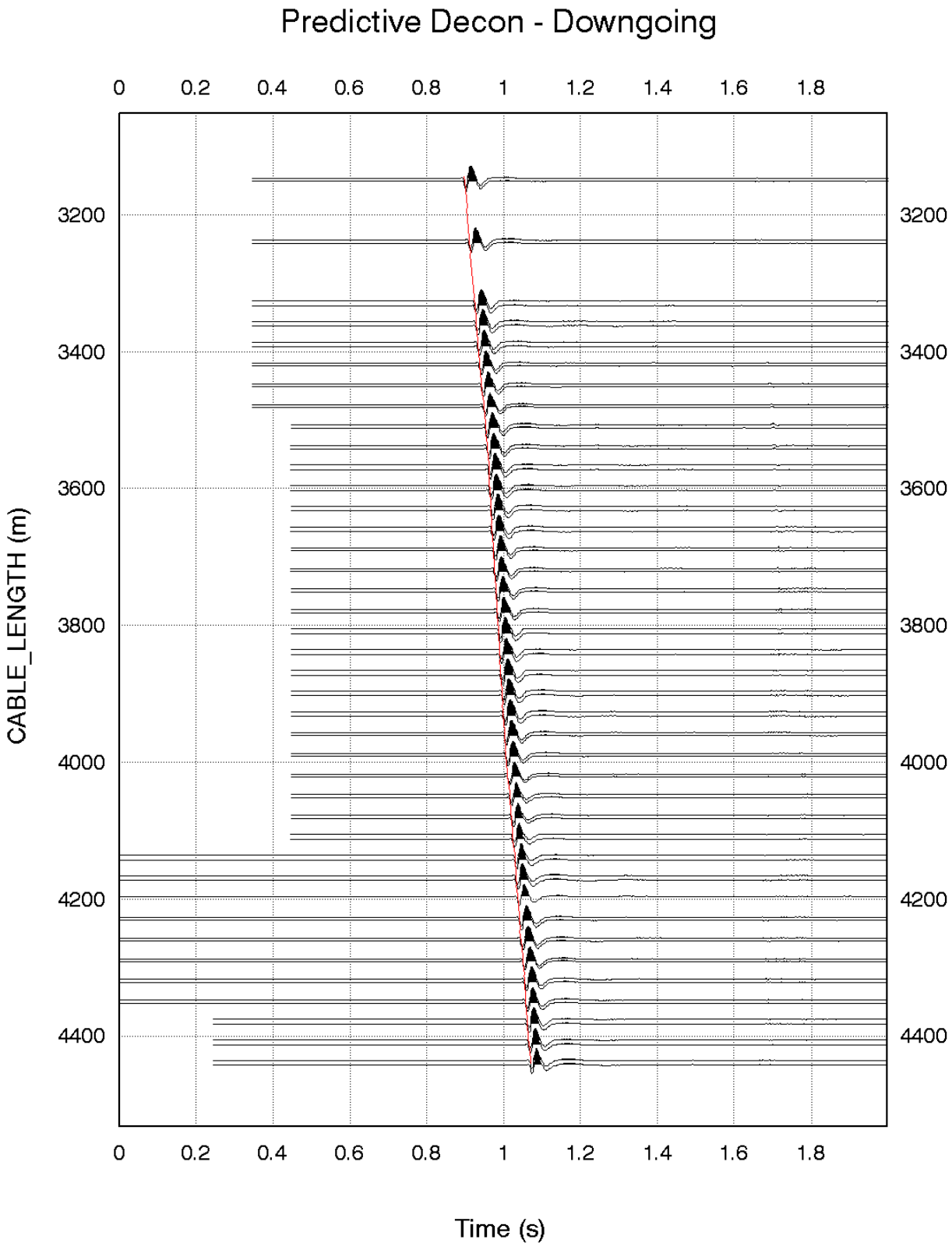

(E) Downgoing wavefiled after predictive deconvolution

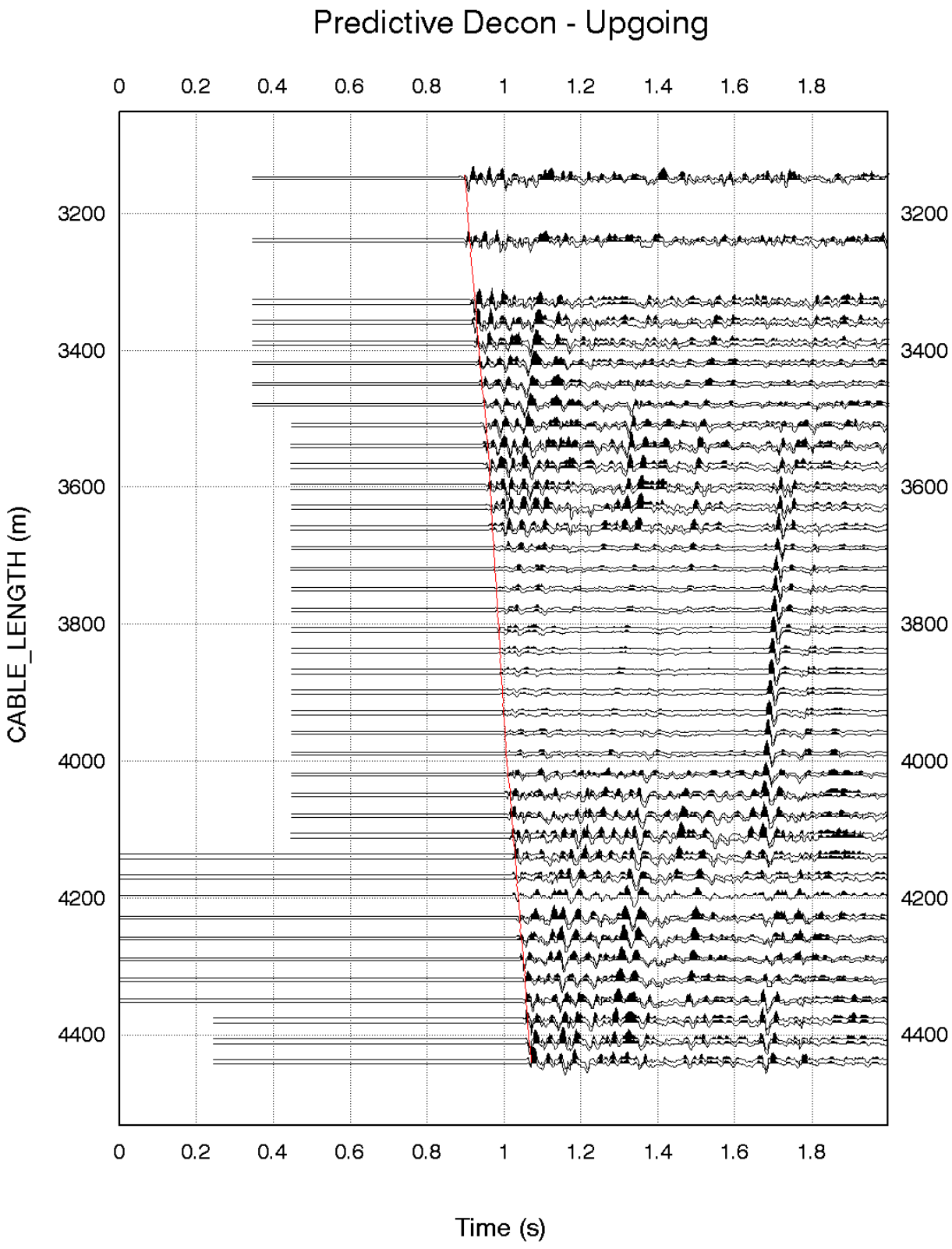

(F) Upgoing wavefield after predictive deconvolution

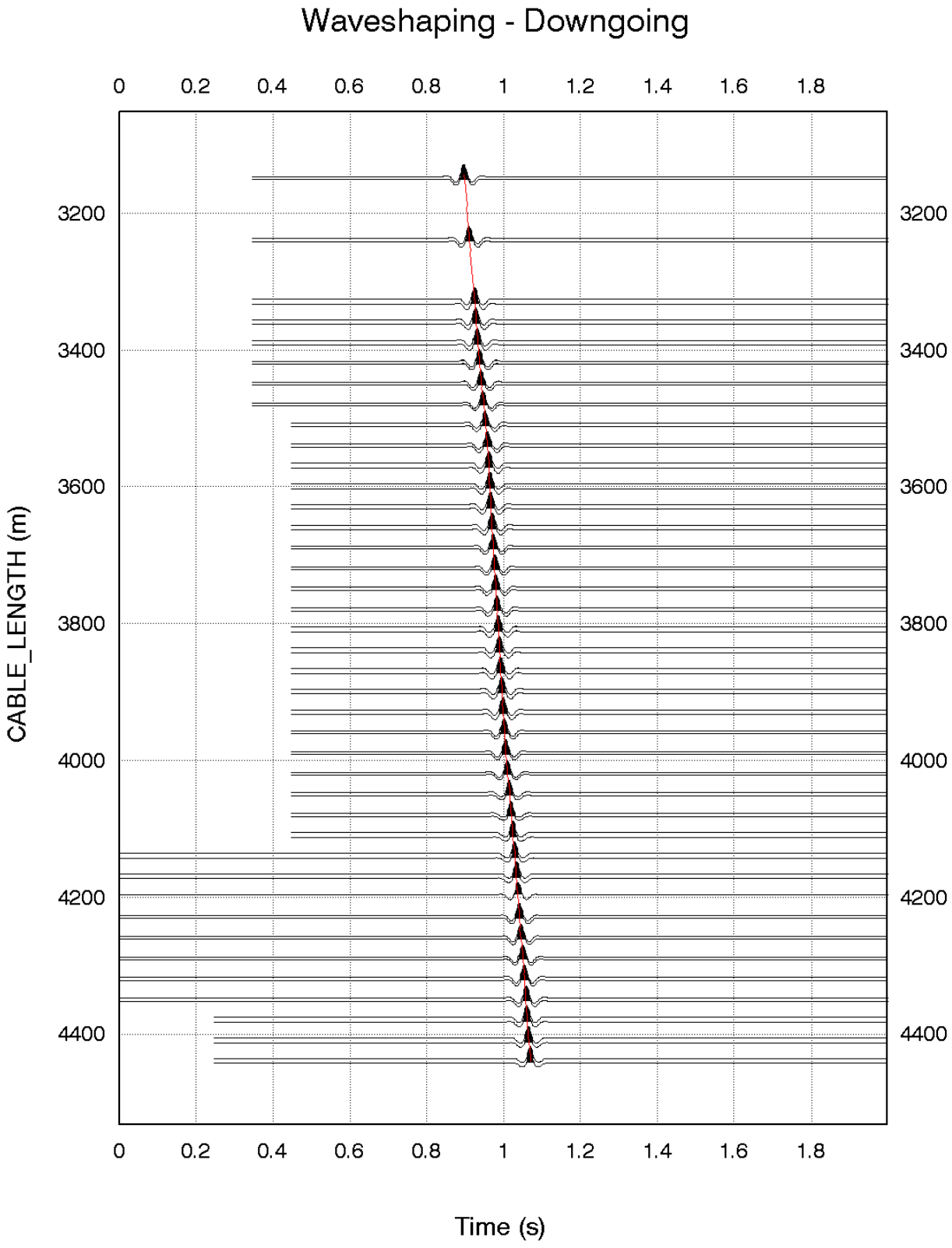

(G) Downgoing wavefield after waveshaping deconvolution

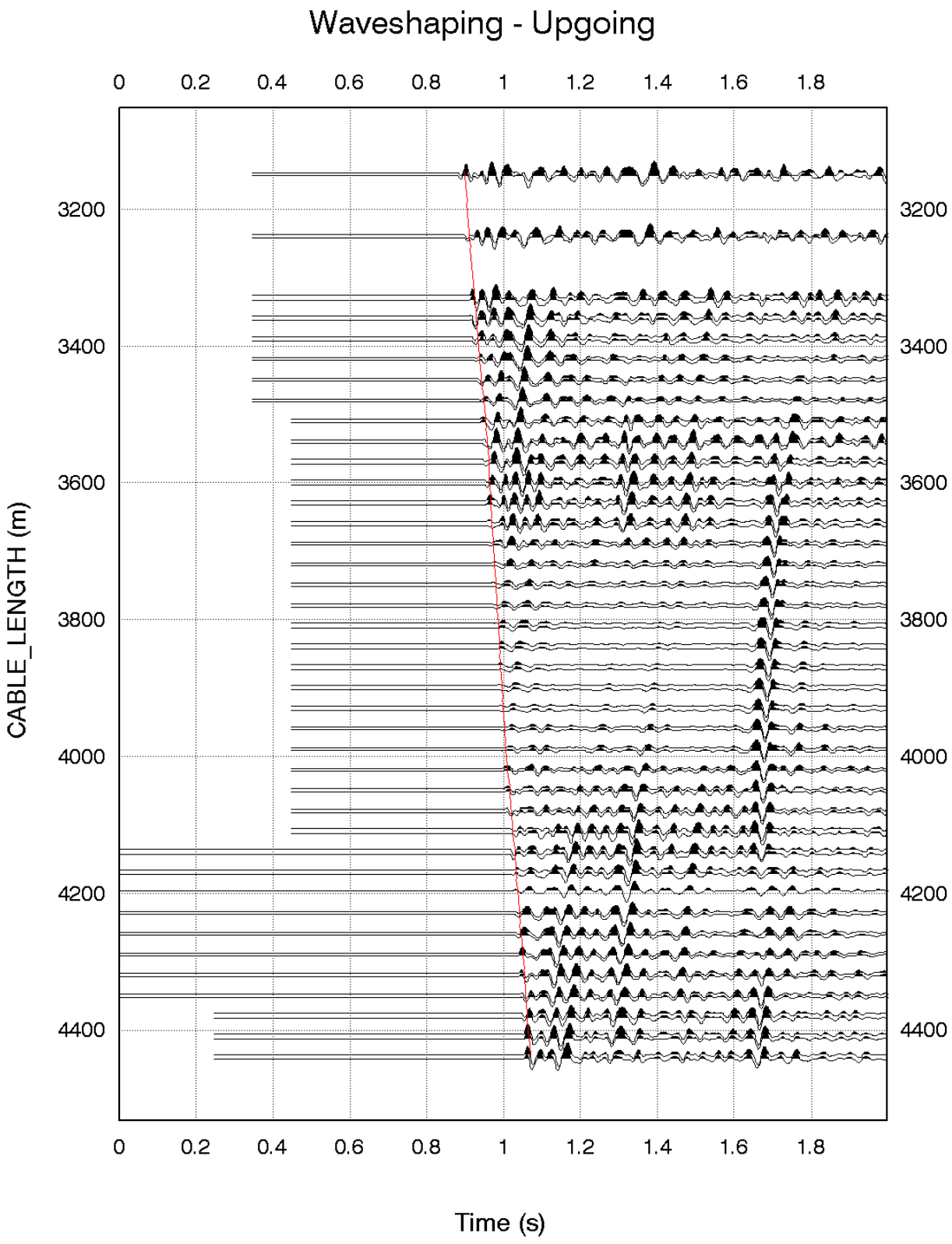

(H) Upgoing wavefield after waveshaping deconvolution

Figure 10 Results of each processing steps for Run-2

4.6 Model building and ray tracing

It was necessary to build an acoustic model of the subsurface for following reasons.

- VSP ray tracing modeling can illuminate a lateral coverage of the subsurface.
- Kirchhoff migration of borehole seismic data requires a background velocity model to guide the migration.

Before the borehole seismic survey, ESSO Australia supplied a 3D model for the area. This 3D model was specified by 12 horizons from the 3D surface seismic interpretation. Interval velocities with lateral variations between these horizons were also given. The base map of the 3D model is shown in Figure 11.

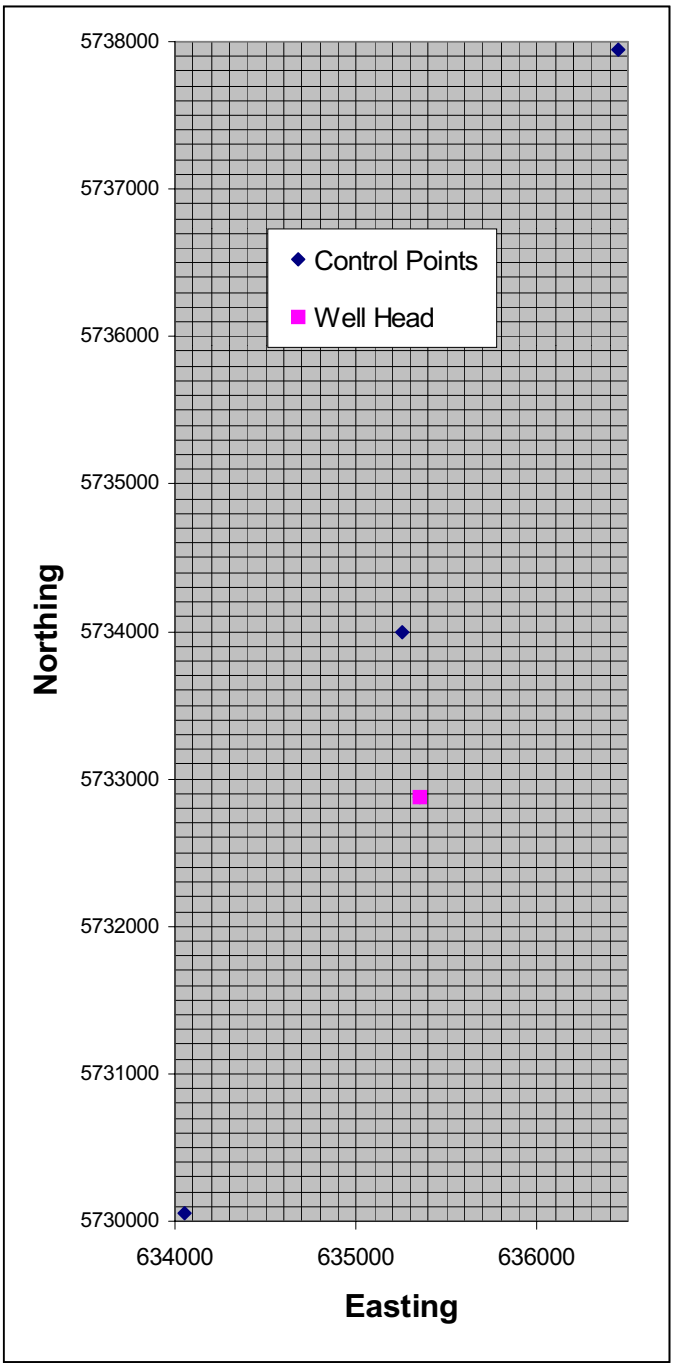

Figure 11 Base map of the 3D model

A 2D vertical cross section along the well trajectory is shown in Figures 12 and 13. The well trajectory projected on the cross section is denoted by the downhole geophone positions. In this 2D section, the origin is at (635305.7E, 5734002.4N). The wellhead is located at (-1130.5, 0). Hereafter, all 2D coordinates are referred to this definition. For simplicity, the interval velocities within each layer were kept constant. These velocities are averages of the interval velocities from the 3D model and listed in Table 4. This velocity model is termed as Model-0.

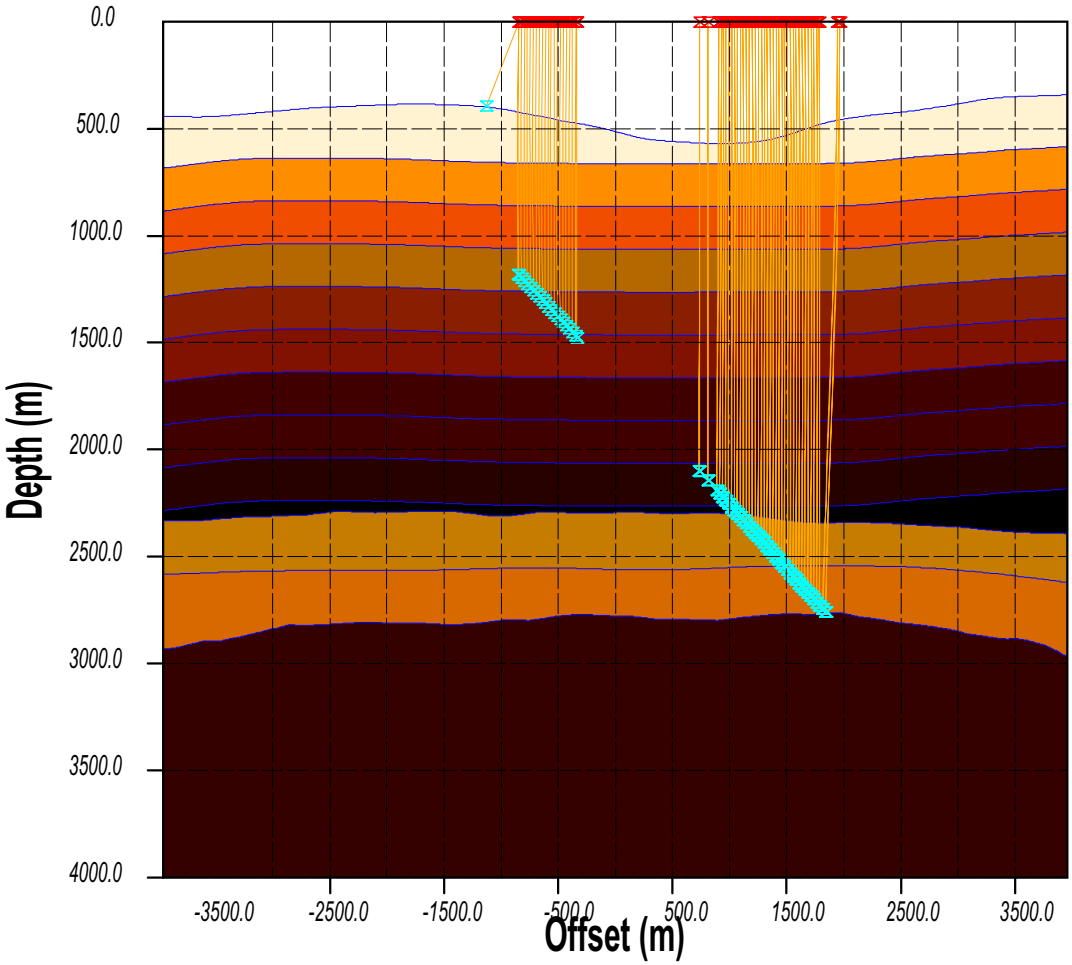

Figure 12 Downgoing P wave rays connecting corresponding sources and receivers in Model-0

Rays were traced between sources and receiver pairs corresponding to the acquisition geometry. In Figure 12, only direct downgoing P wave was considered (PP mode). These rays correspond to the first arrivals on the seismic section. In Figure 13, mode-converted direct downgoing wave was considered (PS mode). In this case, the wave propagated down as compressional wave in the water. Then, it was mode converted to shear at the sea bottom and propagated down to the receivers as shear wave.

More ray bending in PS mode than in PP mode was clearly seen at sections where sea floor is dipping or the source is not directly above the corresponding receivers. This is also reflected by the strength of the shear event mode-converted at the sea floor. In Figure 5A, a shear event mode-converted at the sea floor was clearly visible on Run-1. This event almost disappeared at the shallower section of Run-2 where sea floor is flat, and it re-appeared at the deeper section. In fact,

this event is stronger at the deeper section of Run-2 that that in Run-1 because the sea floor is dipper in the deeper section of Run-2 than the corresponding section of Run-1.

Table 4 Model-0 built from information supplied from ESSO Australia

Layer Name	P velocity (m/s)	S velocity (m/s)	Density (kg/m3)
Water	1500	0	1000
SR27	1676	750	1620
SR28	2423	1200	1751
SR29	2724	1400	1805
SR30	3038	1550	1856
SR31	3289	1650	1893
SR32	3294	1670	1895
SR33	3558	1850	1940
SR34	3491	1820	1940
SR35	3662	1870	1951
BCHAN	3800	2050	2040
MMIO	2983	1550	1850
TLAT	2858	1480	1836
BASE	3800	2100	2100

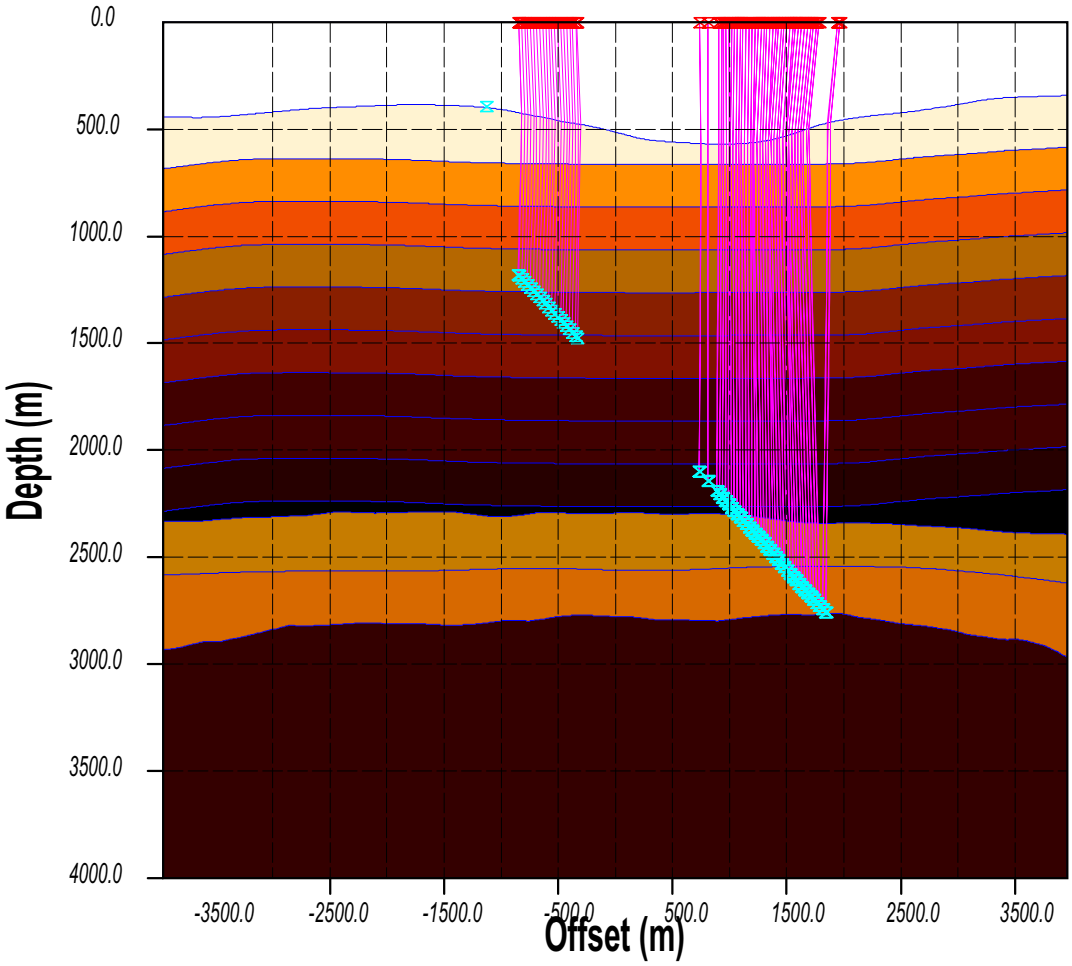

Figure 13 Downgoing mode converted S waves at the sea bottom, rays connecting corresponding sources and receivers in Model-0

4.7 Tomographic inversion of travel times

To verify if Model-0 is a good representative of the local geology, we compare the calculated travel times with the observed travel times for the same source-receiver configuration. The observed transit time is the travel time between the surface hydrophone and the downhole geophone. For the purpose of comparison, therefore, we change the source positions to a depth of 9 m to compensate for the distance between the hydrophone and the airgun. This change is very reasonable considering all source-receiver configurations are almost vertical except for the receiver at the sea floor.

Appendix D lists the source and receiver positions, calculated and observed travel times and the residuals between the calculated and observed travel times. By inspection, it is obvious that there are large positive residuals at the two ends of VIVSP survey and small negative residuals at the middle of the VIVSP survey. The positive residuals indicate that the velocity in the corresponding sections (two ends of the survey) of the model is too slow so that the calculated travel times are greater than the observed travel times. The negative residuals indicate that the velocity in the corresponding section (middle) of the model is too fast so that the calculated travel times are less than the observed travel times.

Table 5 Model-1 obtained from tomographic inversion of travel times

Layer Name	P velocity (m/s)	S velocity (m/s)	Density (kg/m3)
Water	1513	0	1000
SR27	1703	762	1620
SR28	2462	1219	1751
SR29	2768	1422	1805
SR30	3087	1575	1856
SR31	3342	1676	1893
SR32	3347	1697	1895
SR33	3615	1880	1940
SR34	3547	1849	1940
SR35	3721	1900	1951
BCHAN	3861	2083	2040
MMIO	2983	1550	1850
TLAT	2858	1480	1836
BASE	3800	2100	2100

Tomographic inversion of travel times is an optimisation process where the velocity model is systematically updated to minimise the objective function. The objective function is normally a combination of two parts: one is related to the travel time residuals and the other is related to the *a prior* information about the local geology. Here, a simple objective function is defined as

$$F(m) = \sum_{i=1}^{N} (t_{cal}^{i} - t_{obs}^{i})^2 + \text{Re}\, gularization \qquad (2)$$

Here, the regularisation has three parts. The first part involves the acoustic velocity in the water. Here, the transit times between a receiver at the sea bottom and the corresponding transit times were used to determine the water velocity. The acoustic velocity in the water was calculated to be 1513 m/s instead of 1500 m/s, given by ESSO prior to the survey. The second part of the regularisation involves the formations from SR27 to BCHAN. During the inversion, the velocity

ratios among these formations were kept at the same values as those for the original model. The reason behind this is that VIVSP does not have good vertical resolution. The third part of the regularisation involves formations below MMIO. Velocities for formations below MMIO were not changed. After the minimisation of the objective function, a new velocity model, Model-1, was obtained. This new model is tabled in Table 5 and is very close to Model-0.

Rays were traced in Model-1 between sources and receiver pairs corresponding to the acquisition geometry. This time, only reflected events were shown. In Figure 14, both down and upgoing legs were compressional (PP mode). In Figure 15, the downgoing leg was compressional and the upgoing leg was shear (PS mode).

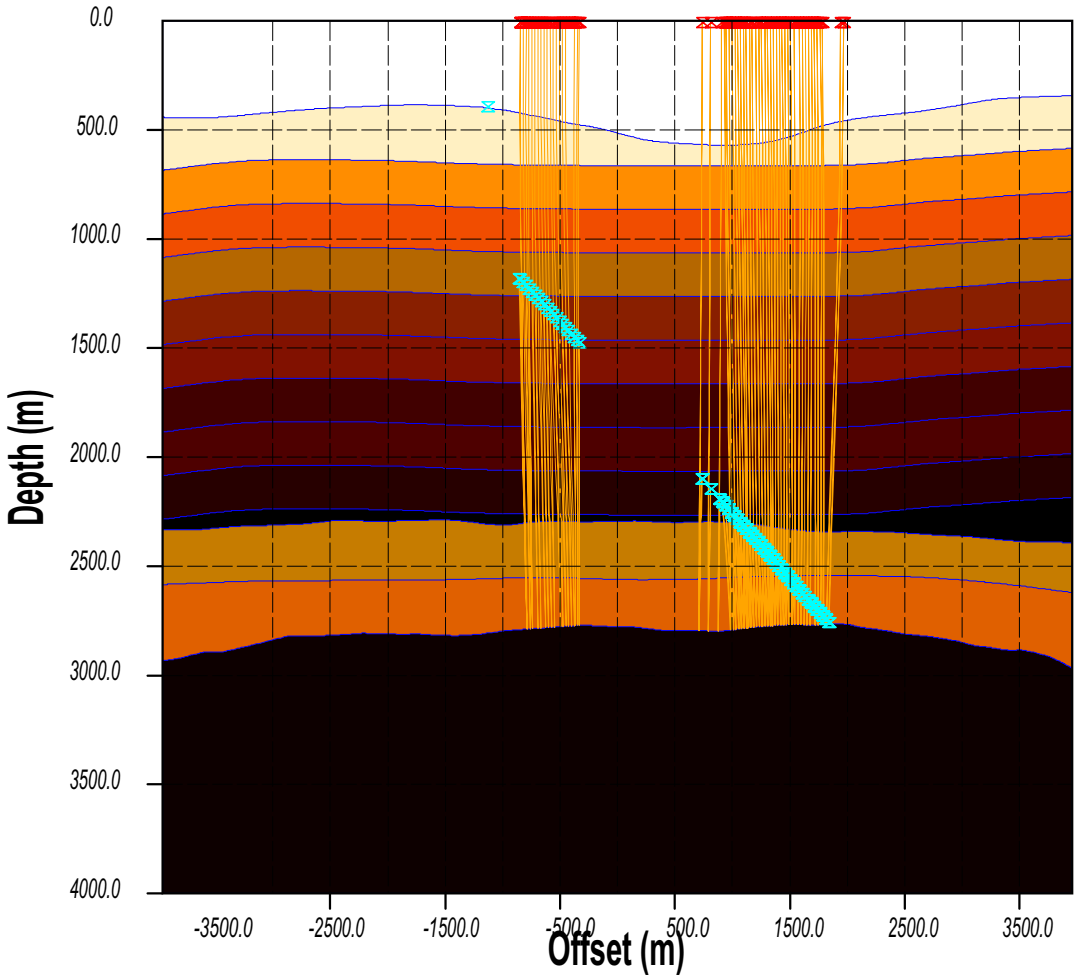

Figure 14 PP reflected rays connecting corresponding sources and receivers in Model-1

Appendix E lists the positions for all source-receiver pairs, the observed direct transit times and the calculated transit times obtained from ray tracing. The residual times are the differences between the calculated and observed times. The mean squared residual times for Model-0 and Model-1 are 17.3 and 12.1 ms, respectively.

An important observation from the variation of the residual times for both Model-0 and Model-1 was that the calculated times at both ends of the survey were greater than those in the middle. This

means that the velocities at both ends of the survey should be greater than those used in the models whereas the velocities in the middle should be less than those used in the models. Unfortunately, this lateral variation was not built into the models.

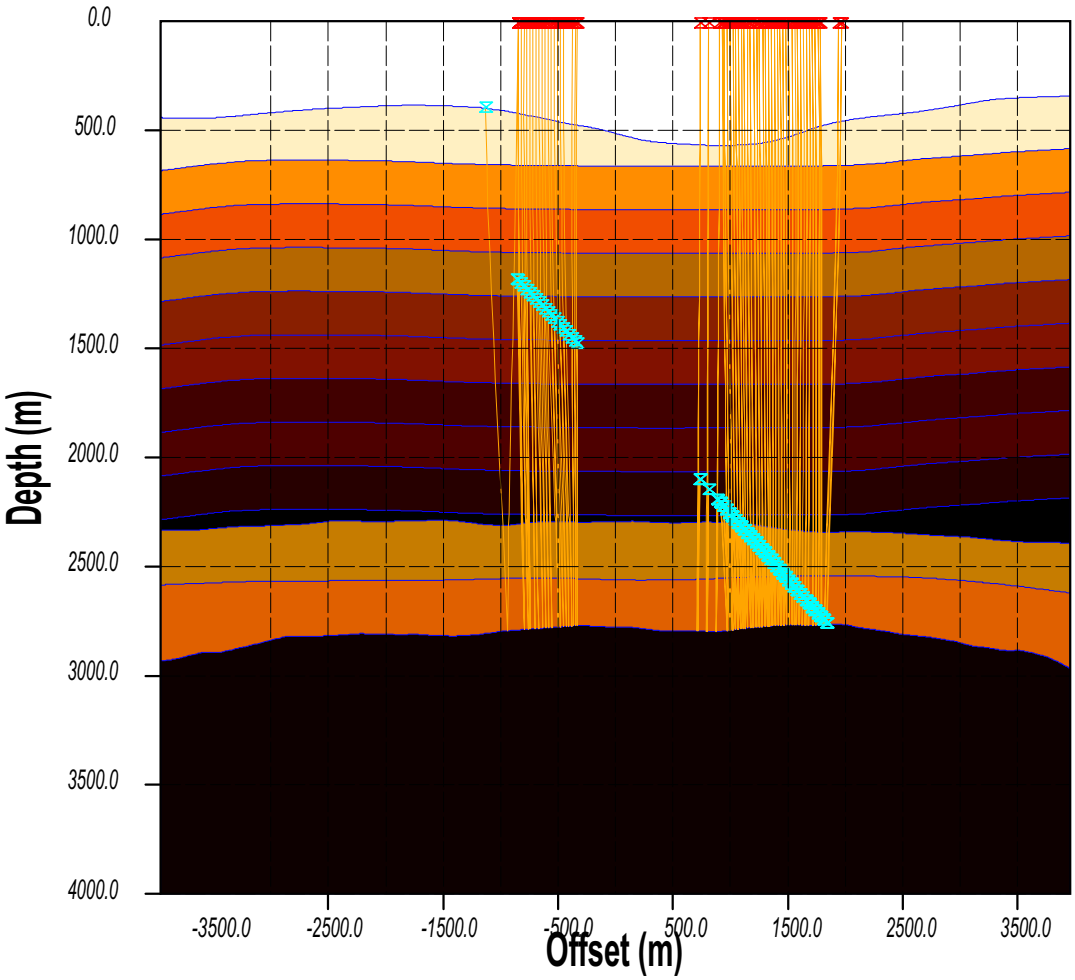

Figure 15 PS reflected rays connecting corresponding sources and receivers in Model-1

4.8 Migration

The purpose of migration is to position the reflected energy contained within the residual wavefield above to its true reflected points (x, y, z) or (x, y, t).

The program used here is a 2D Kirchhoff method and can migrate PP, PS, SP or SS reflections. Both vertical and horizontal input components may be used. In this case the enhanced UP P wavefield was used.

According to the Kirchhoff integral, each point of the subsurface is imaged (migrated) in the following way:

Given the geometry of the survey (relative positions of the sources and the receivers) and a velocity model, the time T_1 is computed to go from the source to one particular point (x, z) in the subsurface.

At this point, the existence of a layer having a local dip of CENDIP-APERT is assumed. Knowing at this point the arrival angle of the ray coming from the source, the Snell's law is applied for the requested code (PP, PS, SP or SS) to compute the departure angle.

Starting from point (x, z), a ray is sent through the model and its intersection with the well (defined by the receiver co-ordinates) is computed. This leads to a time T_2 to go from (x, z) to the well at (x_0, z_0).

Assuming a locally spherical wavefront, the actual arrival time (Ti) of this wavefront is computed on several receivers in the same layer as point (x_0, z_0). At this stage the image is computed by summing the recorded data at times T1+Ti for i receivers (curve T+Ti(z) is generally a hyperbola). This operation is reproduced for a hypothetical reflector at the same point (x,z) having dips ranging from CENDIP-APERT+1 to CENDIP-APERT.

The final value of the image at point (x,z) is the sum for all dips of each estimation damped by a function depending on the distance between the central dip (CENDIP) and the maximum aperture APERT.

The stacking is performed over all traces. If a reflector really exists at that point, the stacked amplitude should be non-zero. If no reflector exists, however, the stacked energy should average out to be zero.

Aperture and Dip:

A prevailing strike and dip (if it is known) of the reflectors to be imaged can be specified. In this case, tomographic inversion results of BBA1ST-1 were used. The maximum dip allowed for a potential reflector was set by the aperture (APERT).

Many tests were run to determine the optimum parameters. The final migration was performed on both Run-1 and Run-2 (Figures 9H and 10H with the parameters described in Table 6.

Table 6. Migration Parameters

Velocity Model	Dip (DEG)	Aperture (DEG)
Model-1	0	+/-7.5

The migration results of both Run-1 and Run-2 are displayed in Figures 16, 17, 18 and 19.

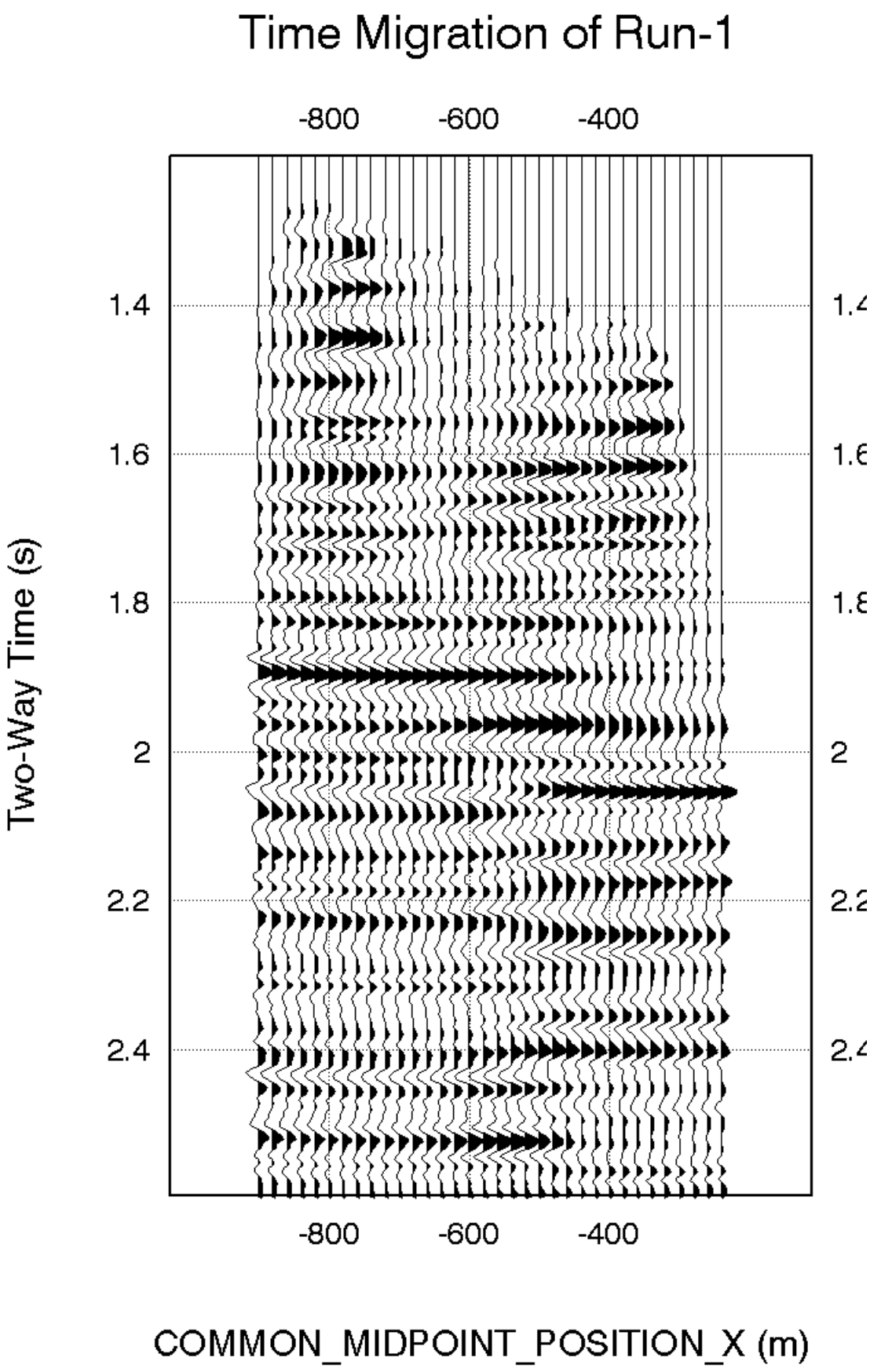

Figure 16. Time migration of Run-1 using Model-1 velocity model

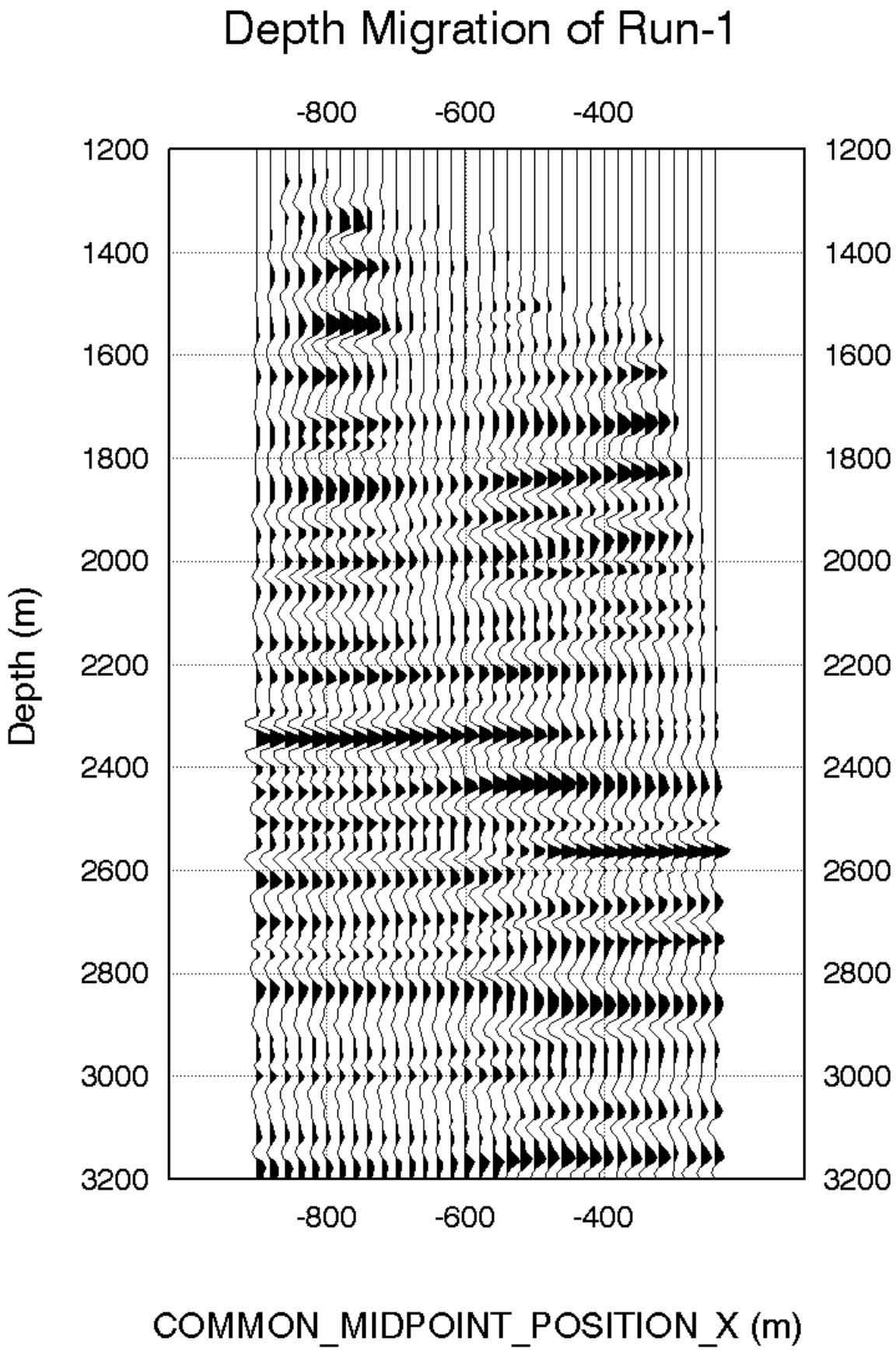

Figure 17. Depth migration of Run-1

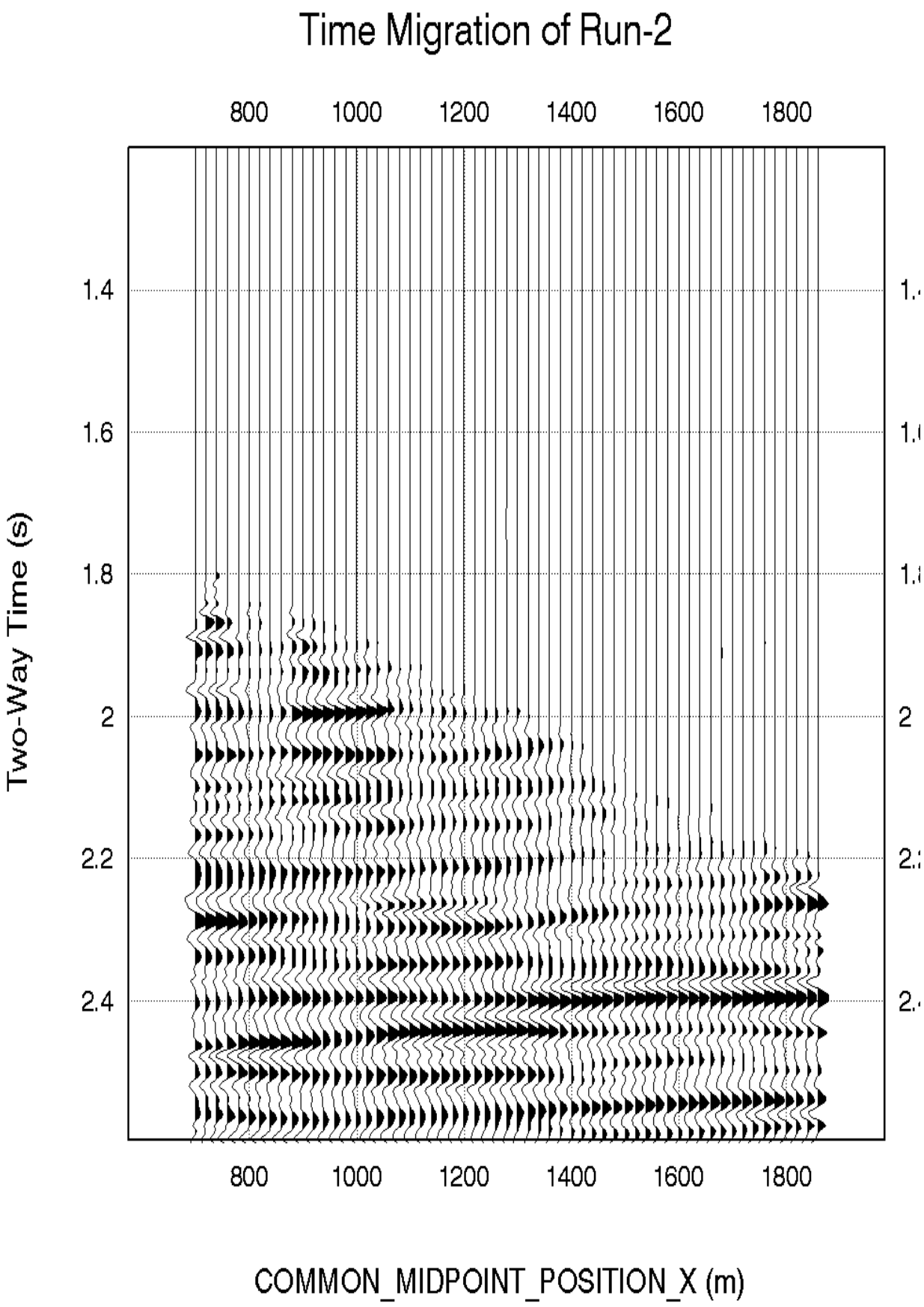

Figure 18. Time migration of Run-2

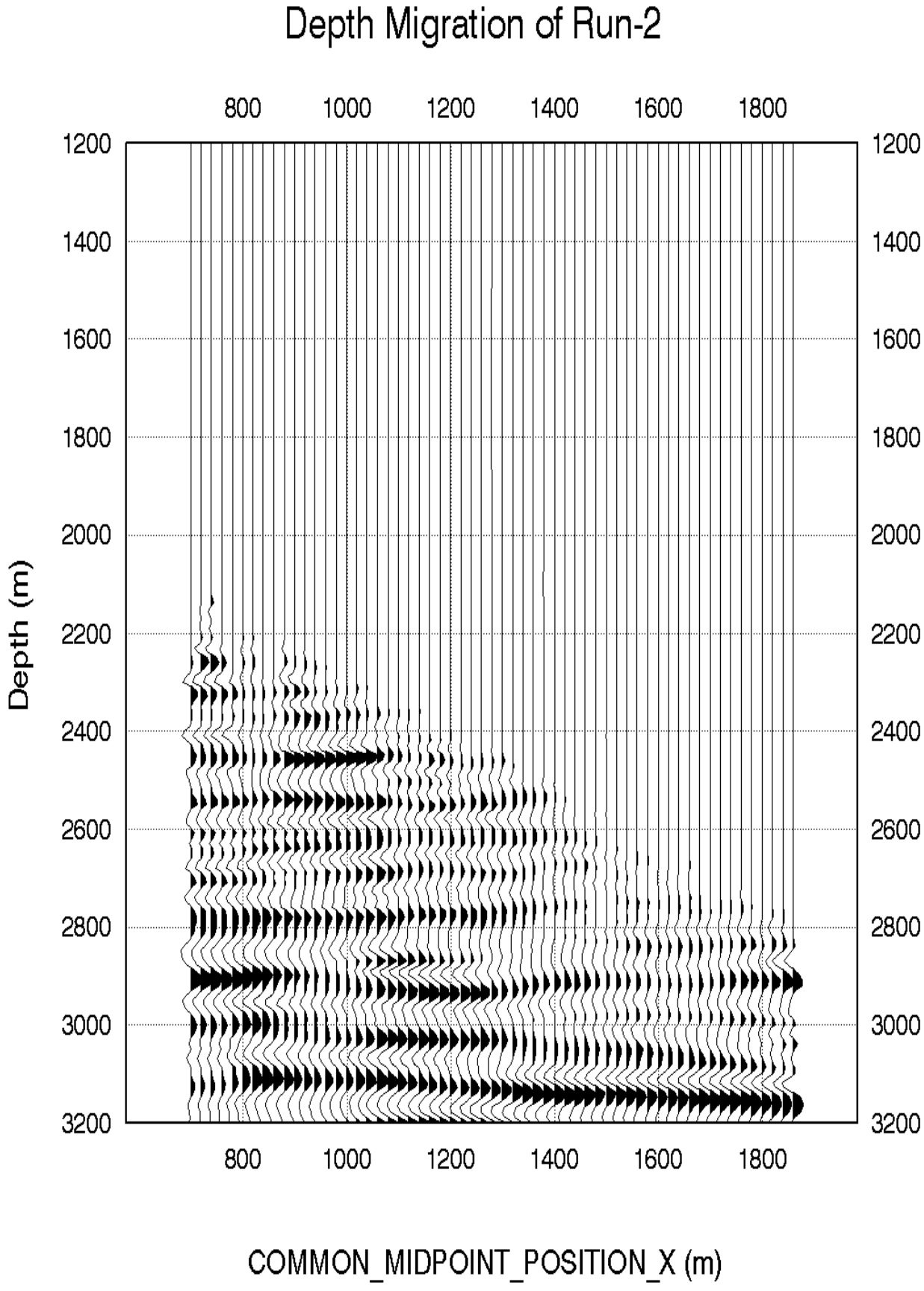

Figure 19. Depth migration of Run-2

A. Well deviation data

B. Raw navigation data and transit times

C. Edited navigation data and re-picked transit times

D. Geophysical airgun report

1. Level number: the level number starting from the top level (includes any imposed shots).

2. Measured depth from KB: the depth in metres from kelly bushing.

3. Vertical depth from SRD: the depth in metres from seismic reference datum.

4. Observed travel time HYD to GEO: the transit time picked from the stacked data by subtracting the surface sensor first break time from the downhole sensor first break time.

5. Vertical travel time SRD to GEO: transit time for the vertical distance between the geophone and the datum after a geometry correction of the observed transit time.

6. Two-way vertical time: two-way vertical transit time between SRD and GEO.

7. Average velocity SRD to GEO: the average seismic velocity from datum to the corresponding checkshot level.

8. Vertical level spacing: the vertical distance between two neighbouring levels.

9. Delta time between levels: the difference of one-way vertical transit time between two neighbouring levels.

10. Interval velocity between levels: the average seismic velocity between two neighbouring levels.

E. Residual times for Model-0 and Model-1